

**EUROPEAN COMMISSION
DG RESEARCH**

**SIXTH FRAMEWORK PROGRAMME
MARIE CURIE RESEARCH TRAINING NETWORKS**



MYMOSA

Motorcycle and motorcyclist safety

Deliverable no.	3.4
Dissemination level	Public
Work Package	WP 3: Personal protective equipment
Author(s)	Mazdak Ghajari, Ugo Galvanetto, Imperial College London
Title	VIRTUAL AND EXPERIMENTAL TESTING OF HELMETS
Status (Final, Draft)	Final
File Name	WP34.pdf
Project Start Date and Duration	01 October 2006 - 30 September 2010



VIRTUAL AND EXPERIMENTAL TESTING OF HELMETS

By:
Mazdak Ghajari and Ugo Galvanetto
Department of Aeronautics
Imperial College London

Abstract

Development and validation of the Finite Element (FE) model of a commercially available helmet in the LS-DYNA crash code is described in this report. For the validation, drop tests were performed at front, rear and side of the helmet onto flat and kerbstone anvils according to the impact absorption test of the UNECE22.05 standard and the same impacts were simulated. Very good agreement was found between the virtual and experimental results for all impacts, except one. The observed discrepancy was attributed to the material model of the shell, which needs further improvements.

The helmet was employed to study the influence of the body on impact responses of the head and helmet. As a human surrogate, the Hybrid III dummy was used. Several drop tests were carried out on the helmeted dummy and the results were used to validate an FE model of the dummy equipped with the model of the helmet; the FE predictions were very good.

Comparison between virtual drop test results of the helmeted Hybrid III dummy and its helmeted detached head indicated that the liner crushing distance was greater in full-body impacts. This can potentially lead to the bottoming out of the foam liner. The solution to an analytical model of the helmeted headform drop test suggested increasing the mass of the head to include the effect of the body in detached-head impacts. The added mass was calculated using the full-body impact results and applied to the Hybrid III headform. The modified head impact results corroborated the idea of the added mass.

TABLE OF CONTENTS

Abstract	2
TABLE OF CONTENTS	3
TABLES	4
FIGURES	4
1 Introduction	5
2 Helmet FE Modelling	7
2.1 Methodology	7
2.1.1 Material properties of foam parts	8
2.1.2 Material properties of composite shell	10
2.1.3 Chin strap	11
2.1.4 Meshing	11
2.1.5 Headform and anvils	12
2.1.6 Contact	13
2.1.7 Helmet drop tests	14
2.2 Results	14
2.3 Discussion	17
3 Helmet Full-body Normal Impact Test Using the Hybrid III Dummy	18
3.1 Methodology	18
3.1.1 FE model of the Hybrid III dummy	18
3.1.2 Full-body and detached-head drop tests	19
3.1.3 Experimental dummy drop tests	20
3.2 Results	24
3.2.1 Experimental dummy drop tests	24
3.2.2 Validating the FE model of the dummy	26
3.2.3 Full-body vs. detached-head drop tests	28
3.2.4 Analytical Model of standard drop test	30
3.2.5 Modified Headform	32
3.3 Discussion	34
4 Conclusions	35
References	37

TABLES

Table 1 Properties of EPS foams (solid polymer density=1050 kg/m ³)	10
Table 2 Material properties of foam parts and chin strap	10
Table 3 Mechanical properties of two laminas of the shell	12
Table 4 Results of dummy drop tests	25
Table 5 Results of drop test simulations	29

FIGURES

Figure 1 Typical engineering stress-engineering strain curve of EPS under compressive loading	8
Figure 2 Shell regions and lay-up; white lines indicate the reference material direction; TW: Twill Weave, H: Hybrid, G: Glass fibre, C: Carbon fibre and PW: Plain Weave. The matrix is epoxy.....	11
Figure 3 Modelled parts of the helmet (only half of the shell is shown) and anvils.....	13
Figure 4 Helmet marking and drop test rigs	14
Figure 5 Results of drop tests at point B	15
Figure 6 Results of drop tests at point P	15
Figure 7 Results of drop tests at point R.	15
Figure 8 Results of drop tests at point X.	16
Figure 9 Snapshots of an impact onto kerbstone anvil at point R.	16
Figure 10 Hybrid III dummy (left) and its FE model (right).....	18
Figure 11 Helmeted Hybrid III dummy (left) and helmeted detached head of the dummy (right) impacting the anvil at point B.....	20
Figure 12 Base, load-cell and anvil (left) and connection of beams to the ground (right).....	21
Figure 13 The suspended dummy (left) and the bomb release (right).	21
Figure 14 Adjustment of the drop height (left) and the impact point (right).....	22
Figure 15 Impact configurations.	22
Figure 16 Speed measurement.	23
Figure 17 Head and neck instrumentation.....	24
Figure 18 Positive directions of angular acceleration and force and moment components (only half of the helmet is shown).....	24
Figure 19 Snapshots showing slightly missed impacts (left) and accurate impacts (right).	26
Figure 20 FEA results of the AGV-T2 helmet front impact onto a flat anvil at a 6 m/s impact velocity using a Hybrid III dummy compared with the experimental results for the same impact, shown as dashed curves.....	27
Figure 21 Movement of the body in the front impact test, compared with the FEA; a) 0 ms, b) 4 ms, c) 8 ms and d) 12 ms.	28
Figure 22 Results of full-body and detached-head drop tests at 6 m/s.	29
Figure 23 Results of full-body and detached-head drop tests at 7.5 m/s.....	30
Figure 24 Added mass index for the helmeted dummy drop test (left) and comparison of the results using $\gamma_m=0.43$ (right); at a 7.5 m/s impact velocity.	33

1 Introduction

Motorcyclists are among the most vulnerable road users. In Europe they account for 16% of total road-user fatalities (COST327, 2001), even though motorcycles comprise only 6.1% of all motorised vehicles in Europe (ACEM, 2006). Head injury is the most frequent type of injury that causes death or disability in motorcycle accidents, and the only piece of protective equipment that protects the head is the safety helmet. The results of a statistical investigation on motorcycle accidents in the US from 2000 to 2002 revealed that about 51% of unhelmeted riders suffered head injuries as compared to 35% of helmeted riders (NCSA, 2007). Given the fact that motorcycles are much less stable than four-wheel vehicles and their riders can become separated from the vehicle in an accident, the variety of impact configurations for motorcyclists is enormous. Therefore it is difficult to define a limited number of realistic test conditions for evaluating the protective capability of helmets.

A survey of the history of helmet standards revealed that the test method for evaluating the energy absorption capacity of helmets has evolved considerably (Becker, 1998). The first standards adopted a simple method; the helmet was positioned on a fixed headform and impacted with a striker. Among the disadvantages of this method was using a fixed headform, while in real world accidents a moving head impacts another object. Current standards require dropping a helmeted headform on a rigid anvil at a specific impact velocity (Ghajari, et al., 2008). The helmet passes the standard if the resultant linear acceleration of the headform is lower than a given limit. For example, the ECE 22.05 regulation (UNECE22.05, 2002) requires dropping helmeted headforms at 7.5 m/s onto flat and kerbstone anvils. The pass/fail criteria are a 275g peak linear acceleration and a value of 2400 for *HIC* (Head injury Criterion). Although the test method has improved, it is still far from representing real world accidents, where the whole body is present.

In an attempt to study the performance of helmets in more realistic test conditions, an Ogle OPAT dummy was supported at its torso and the side of its helmeted head was impacted with a flat striker (Gilchrist and Mills, 1996). The dummy's neck was replaced with a more flexible neck made of plates connected with pins. The rotational stiffness of the new neck was 0.53 Nm/degree, which was approximately 10 times lower than the rotational stiffness of the Hybrid III dummy's neck. It was found that the peak striker force was 10% higher than the product of the peak resultant linear acceleration of the head and its mass, which was a result of the head/torso coupling through the neck. One drawback of this study was hitting the still headform with a striker, which almost never occurs in real world motorcycle accidents. In addition, only the side impact with a zero degree body impact angle (the angle between the body longitudinal axis and the surface of the opposite object) was tested, while accidents occur at various body impact angles.

Other studies have reported the use of anthropomorphic test devices (ATD) in helmet drop tests. Aldman et al. (Aldman, et al., 1976, Aldman, et al., 1978a, Aldman, et al., 1978b) dropped a helmeted Ogle-Opat dummy onto a surface made of asphalt concrete at 4.4 m/s and 5.2 m/s impact speeds, and measured the linear and rotational accelerations of the head. In a similar research study (COST327, 2001), a pedestrian Hybrid III dummy and its detached head were fitted with helmets and dropped onto flat anvils, and the linear and rotational accelerations of the head were recorded. The impact configurations were front/30° (impact site/body impact angle), crown/90° and rear/30°. Impact speeds of 4.4, 5.2 and 6 m/s were chosen "to simulate realistic impact conditions and to limit the risk of severe damage to the dummy". It was concluded that "the effect of the body and the neck is thus a decrease of the measured linear acceleration values when compared with headform

Project: MRTN-CT-2006-035965 MYMOSA

Deliverable 3.4: Virtual and experimental testing of helmets

measurements". However, the crushing distance of the liner, which is a crucial design parameter, was not reported and compared in that study.

Due to the risk of damage to expensive equipment such as dummies, some impact events cannot be studied experimentally. Instead, validated finite element (FE) models can be used to investigate them. In this report, the FE modeling and validation of a commercially available helmet is presented. This model is used later to simulate full-body and detached-head impacts, using FE models of the Hybrid III dummy and its head. One aim of the study is to investigate the effect of the body on acceleration of the head and also crushing distance of the liner. Another aim is to find a simple yet appropriate way to include this effect in helmet drop tests.

2 Helmet FE Modelling

FE models are capable of predicting very complicated mechanical phenomena that occur when crushing a helmet, such as material non-linearity, large deformation and contact. This capability has made them indispensable to helmet modelling. Among the first FE models was the model of an open-face helmet developed by Yettram et al. (1994). It was used to study the influence of the material properties of the foam and shell on head acceleration but only impacts at the crown site were simulated. A more advanced model was developed to study the fit effect of helmets (Chang, et al., 2001) and the protective capability of the chin bar of full-face helmets (Chang, et al., 2000). In that model, contact elements were inserted at the head/liner interface and the shell and liner were connected through common nodes. Different materials were considered for the shell, including the ABS (acrylonitrile butadiene styrene copolymer), PC (polycarbonate) and a glass fibre reinforced polymer. A bilinear kinematic hardening plasticity material model was used for the shell, even when it was made of a composite material. The helmet model with an ABS shell was validated against drop tests onto a flat anvil at crown, side and rear sites.

Composite materials have a significant number of failure modes, which probably is the reason that composite shells are able to absorb a greater portion of the impact energy compared to conventional thermoplastic shells. Hence, a suitable material model should be used for them in FE models. In a paper by Kostopoulos et al. (2002), the impact response of a composite shell helmet dropped onto a hemispherical anvil at the crown site was studied by using the FE method. One important feature of their model was simulating delamination. Adjacent nodes of the shell layers were tied together until the interaction stresses satisfied a quadratic delamination condition. They also implemented three failure modes for the woven fabric layer of the shell: fibre tensile, matrix tensile and matrix compressive failure. This model, however, was not validated against experiments.

Another attempt to model a composite shell helmet was made by Aiello et al. (2007). They FE modelled a commercially available helmet and validated it against experimental drop test results. Nonetheless, the failure modes assumed for the shell were not described properly. In addition, the sensitivity of the results to mesh size and type of elements were not addressed. Cernicchi et al. (2008) investigated the mesh sensitivity issue but they used an elastic-plastic material model for the shell. They developed an FE model of a commercially available composite shell helmet. The model gave acceptable predictions of experimental drop test results.

In this section, the FE modelling of a commercially available helmet is described and experimental drop tests are simulated in order to validate the model. This helmet is used later to simulate full-body drop tests in order to study the influence of the body on head and helmet impact responses in helmet drop tests.

2.1 Methodology

A recently designed helmet, which is called AGV-T2 in this report, was provided by Dainese S.p.A. (within the EU MYMOSA network) for full-body drop tests using the Hybrid III dummy (explained later). The size of the helmet was 57-58 cm. In spite of belonging to the AGV racers' range, this helmet is representative of a number of commercially available helmets, which have a composite shell and a liner made of Expanded Polystyrene (EPS). In addition, the high energy absorption capacity of the helmet reduced the risk of damaging the dummy in drop tests.

Similar to other helmets, the AGV-T2 helmet has a protective padding or liner, shell, chin strap, comfort padding and visor. The liner is composed of the main foam, top foam, cheek foam and chin foam (foam parts). The liner and the shell are the

components that absorb the impact energy. They were modelled as well as the chin strap. By contrast, the visor and comfort padding do not contribute to energy absorption and therefore they were not modelled.

2.1.1 Material properties of foam parts

The foam parts of the helmet are made of EPS. EPS belongs to the category of closed-cell polymeric foams that collapse plastically when compressed beyond their elastic regime. Therefore, three regimes are distinguishable in its compressive stress-strain characteristic curve as shown in Figure 1. The first regime, which is linear elastic and more extended (up to 5% strain) compared to metals, is characterized by Young's modulus (E) and Poisson's ratio (ν). Young's modulus of EPS is a function of its relative density as (Gibson and Ashby, 1999):

$$E = AR^2 + BR \quad (1)$$

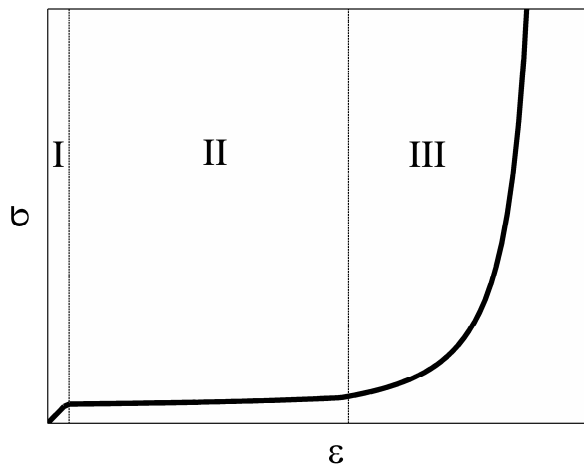


Figure 1 Typical engineering stress-engineering strain curve of EPS under compressive loading.

where A and B are material constants and R is the foam relative density defined as the foam density divided by the solid polymer density. By curve fitting to the results of compressive loading of EPS samples with different densities, the material constants $A = 6640$ MPa and $B = 25.8$ MPa were found (Cernicchi, et al., 2008). Poisson's ratio does not have a significant relation with the relative density. An investigation of the *crushable foam* material model (MAT63) of LS-DYNA (Hallquist, 2007), which was used for the foam parts, revealed that under a compressive load Poisson's ratio remains effective even beyond the elastic regime, while EPS does not deform laterally beyond this regime. Since the elastic regime is negligible compared to the plateau regime, this constant was set to a very small value (0.01).

The plastic collapse of cells comprising the foam results in the long plateau of the curve depicted in Figure 1 (region II). This part of the curve can be fitted with the following equation:

$$\sigma = \sigma_y + \frac{p_0 \varepsilon}{1 - \varepsilon - R} \quad (2)$$

where σ and ε are the compressive engineering stress and strain (Mills and Gilchrist, 2008). σ_y is the yield stress and p_0 is the initial gas pressure, which is usually equal to the atmospheric pressure (0.1 MPa). Experimental investigations have shown that the yield stress can be described with:

$$\sigma_y = CR^{1.5} \quad (3)$$

where C is a material constant (Gilchrist and Mills, 1994). Cernicchi et al. (2008) extracted this constant through curve fitting to the results of dynamic tests on EPS foams with various densities, conducted by Di Landro et al. (2002). In these tests, EPS samples were impacted with a flat object at a 2.1 m/s impact speed. However, helmets are usually tested at speeds higher than 6 m/s, at which the strain rate effect of the EPS is not negligible. Therefore, the quasi-static compression test data reported in (Di Landro, et al., 2002) for EPS foams were used to calculate C . This constant was then increased by 20% to take into account the strain rate effect at helmet drop test speeds, as suggested by (Mills, et al., 2009). At the end a value of 48.3 MPa was found for C .

Young's modulus and the yield stress of two EPS foams with different densities were computed using eqs. (1) and (3) and compared to the experimental data reported in (Mills, et al., 2009), as presented in Table 1. The results show that the equations can estimate these mechanical properties with an acceptable degree of accuracy.

Excessive compression of EPS causes cell walls to crush together, which results in the steep rise of the stress when increasing the strain to a limiting strain ε_D . It forms the third part of the curve shown in Figure 1. This behaviour is best described by:

$$\sigma = \frac{1}{D} \left(\frac{\varepsilon_D}{\varepsilon_D - \varepsilon} \right)^m \left(\sigma_y + \frac{p_0 \varepsilon}{1 - \varepsilon - R} \right) \text{ when } \varepsilon > \varepsilon_D \left(1 - \frac{1}{D} \right) \quad (4)$$

where D and m are material constants (Gibson and Ashby, 1999). $D = 2.3$ and $m = 1$ for plastic foams. The full densification strain is well described by:

$$\varepsilon_D = 1 - 1.4R \quad (5)$$

In our work, the EPS foams of the helmet were modelled with MAT63. The required inputs of this material model are Young's modulus, Poisson's ratio and a compressive stress-strain curve, which were obtained by using eqs. (1) to (5) and are presented in Table 2.

Table 1 Properties of EPS foams (solid polymer density=1050 kg/m³)

	Density (kg/m ³)	R	E (MPa)	σ_y (MPa)
Test (Mills, et al., 2009)	22	0.021	3.0	0.14
eqs (1) and (3)			3.5	0.15
error			17%	7%
Test (Mills, et al., 2009)	59	0.056	19	0.62
eqs (1) and (3)			22.4	0.64
error			18%	3%

Table 2 Material properties of foam parts and chin strap

Part	ρ (kg/m ³)	E (MPa)	ν	σ_y (MPa)
EPS top	20	2.9	0.01	0.13
EPS main	40	10.6	0.01	0.36
EPS cheek and chin	60	23.2	0.01	0.66
Chin Strap	870	1000	0.3	-

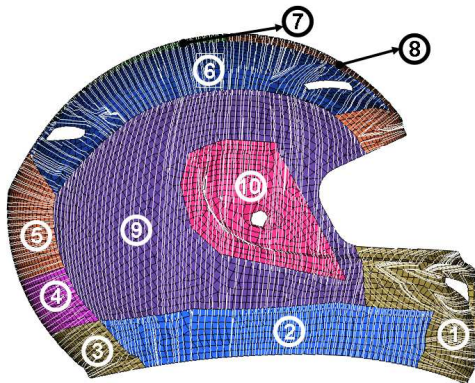
2.1.2 Material properties of composite shell

The shell of the AGV-T2 helmet is made of a number of composite layers. According to the information provided by the helmet manufacturer, the constituents of these layers are Kevlar 49 fibres, carbon (T700) fibres, glass fibres and an epoxy resin. However, these data were not enough to model the shell in LS-DYNA. To obtain more information, six samples were cut from chin bar, side, rear inferior, rear superior, crown and front regions of the shell (Figure 2). They were moulded in resin, polished and inspected under a microscope. The observations suggested that five different laminas were used in the shell: a Kevlar/carbon/epoxy hybrid unidirectional (UD) lamina, a glass/epoxy twill weave woven lamina, a glass/epoxy UD lamina, a plain weave woven lamina and a carbon/epoxy UD lamina. The microscopy images were further processed using the microscope's software. The outcomes were approximate thicknesses and fibre volume fractions of the laminas as well as lay-up of the shell at different regions, reported in Figure 2.

Material properties of the shell laminas were found in manufacturers' databases or obtained from the properties of their constituents using the method explained in (Cernicchi, et al., 2008). One part of the shell section is a hybrid UD lamina. The hybrid lamina is made of strips of a carbon (T700)/epoxy UD composite and a Kevlar 49/epoxy UD composite. To obtain material properties suitable for insertion in the FE model of the shell, it was assumed that the hybrid lamina is in-plane homogenous. Its mechanical properties were calculated from the properties of its constituents by using

the rule of mixtures and making some assumptions about failure modes. Then, its properties were validated by carrying out coupon tests and comparing the results with FE predictions. Mechanical properties of the shell layers are presented in Table 3.

The shell of the AGV-T2 helmet was modelled with the *Laminated Composite Fabric* material model (MAT58) of LS-DYNA. This material model is capable of predicting initiation and evolution of intra-laminar damage. It is also suitable for modelling UD and woven composites. Delamination was not modelled because it could have a drastic effect on the computational cost.



- 1, 2 and 3) chin bar: $[(0_{TW,G})_2/\pm 30_H/(\pm 30_G)_2]$
 4) rear inferior: $[0_{TW,G}/\pm 30_H/(0_C/90_C)_4/(\pm 30_G)_2]$
 5) rear superior: $[0_{TW,G}/(\pm 30_H/\pm 30_G)_2/0_{PW,G}/\pm 30_G]$
 6) vent: $[0_{TW,G}/(\pm 30_H)_2/(\pm 30_G)_5/0_{PW,G}/\pm 30_G]$
 7) crown:
 $[0_{TW,G}/(\pm 30_H)_2/(\pm 30_G)_2/(\pm 30_H)_2/(\pm 30_G)_2/0_{PW,G}/\pm 30_G]$
 8) front: the same as 5.
 9) side: $[0_{TW,G}/\pm 60_H/(\pm 30_G/\pm 30_H)_2/\pm 30_G/\pm 60_G/\pm 60_H/\pm 60_G/0_{PW,G}/\pm 60_G]$
 10) side patch:
 $[0_{TW,G}/(\pm 30_G/\pm 60_G)_2/\pm 30_G/\pm 60_H/\pm 60_H/\pm 30_G/\pm 30_H/(\pm 30_G)_2/\pm 30_H/(\pm 30_G)_2/\pm 60_H/(\pm 60_G)_2/\pm 60_H/\pm 60_G/0_{PW,G}/\pm 60_G]$

Figure 2 Shell regions and lay-up; white lines indicate the reference material direction; TW: Twill Weave, H: Hybrid, G: Glass fibre, C: Carbon fibre and PW: Plain Weave. The matrix is epoxy.

2.1.3 Chin strap

The 1.3 mm thick and 20 mm wide chin strap of the helmet was modelled with the *Elastic* material model. Its properties are presented in

Table 2. The Young modulus was set equal to the value obtained from a tension test on a chin strap (Mills and Gilchrist, 2008).

2.1.4 Meshing

CAD files of the shell and foam parts were provided by Dainese S.p.A. in the IGS format. These files were imported into the Hypermesh environment (2008), where the surfaces constructing the shell and foam parts were prepared for mesh generation. The preparation process included stitching the edges where there was a gap and removing the lines which could cause very small element edges and therefore a small time step.

The foam parts were meshed with single integration 4-node tetrahedral elements. The tetrahedron is suitable for mesh generation on complicated volumes such as a helmet liner, but it is susceptible to excessively stiff behaviour (locking) (Cook, 2001). A good replacement for this element is the 8-node hexahedron but it is very difficult to

properly discretize the liner using hexahedrons. It is, however, possible to compare the performance of these elements in the type of problem under investigation. Cernicchi et al. (2008) simulated the crushing of an EPS mat impacted with a 3 kg rigid sphere at an impact speed of 6.7 m/s. The EPS foam, which had a density of 24 kg/m³, was modelled using MAT63. They found that when 4-5 tetrahedrons were used through the thickness, the acceleration of the impactor versus time converged to that obtained by using the same number of hexahedrons through the thickness. This evidence together with their validation results of the whole helmet verifies that the 4-node tetrahedron is suitable for meshing the liner if at least four elements exist through its thickness. Following this suggestion, the liner of the AGV-T2 helmet was meshed with 39836 4-node tetrahedrons.

The shell was meshed mainly with 4-node quadrilateral elements. They composed 95% of the elements of the shell. In some complex areas, 3-node triangular elements were employed. Average element size was 3 mm following the suggestions of Cernicchi et al. (2008). Each layer of the shell was represented with a through thickness integration point and pertinent material properties were assigned to this point.

Table 3 Mechanical properties of two laminas of the shell

	glass/epoxy twill weave ($V_f = 0.55$)	glass/epoxy UD ($V_f = 0.6$) (Soden, et al., 1998)	polymer fibre/epoxy ($V_f = 0.4$)	carbon/ epoxy ($V_f = 0.5$)	hybrid (carbon/epoxy – Kevlar49/epoxy)
ρ (kg/m ³)	1950	1984	1266	1455	1400
E_L (GPa)	29	46	34	174	110
E_T (GPa)	29	16	8	9	8
G_{LT} (GPa)	4.1	5.8	1.8	3.9	2.8
ν_{LT}	0.14	0.28	0.37	0.29	0.33
$S_{ut,L}$ (MPa)	550	1280	840	2000	1530
$\epsilon_{ut,L}$	0.019	0.028	0.026	0.014	0.014
$S_{uc,L}$ (MPa)	490	800	126	1420	720
$\epsilon_{uc,L}$	0.017	0.018	0.020	0.010	0.008
$S_{ut,T}$ (MPa)	550	40	52	42	30
$\epsilon_{ut,T}$	0.019	0.025	0.014	0.009	0.004
$S_{uc,T}$ (MPa)	490	145	130	130	130
$\epsilon_{uc,T}$	0.017	0.012	0.016	0.014	0.015
τ_u (MPa)	80	73	60	60	60
γ_u	0.04	0.040	0.051	0.051	0.051

2.1.5 Headform and anvils

The CAD file of a “J” size ISO headform was imported into Hypermesh and meshed with 37550 tetrahedrons. The mesh was imported into LS-DYNA and a rigid material

with a density of 1173 kg/m^3 was assigned to it. The mass of this headform was measured at 4.727 kg , which is within the range of the mass defined by UNECE 22.05, $4.7 \pm 0.14 \text{ kg}$. Its centre of gravity was in the mid-sagittal plane and about 5 mm away from the point G, where the accelerations are measured. According to the UNECE 22.05 standard, the centre of gravity shall be near this point.

The AGV-T2 helmet was positioned on the headform, considering the upper and lower vision field angles defined in UNECE 22.05. The chin strap was passed through the hole of the cheek foam and below the neck, as shown in Figure 3. In a simulation, the chin strap was tightened with a 5 N force. Then, the nodes and elements were imported into the main model without pre-stress.

Flat and kerbstone anvils were created in Hypermesh software. They were meshed with shell elements and imported into LS-DYNA (Figure 3). A rigid material with a Young's modulus of 200 GPa (typical of steel) was assigned to them.

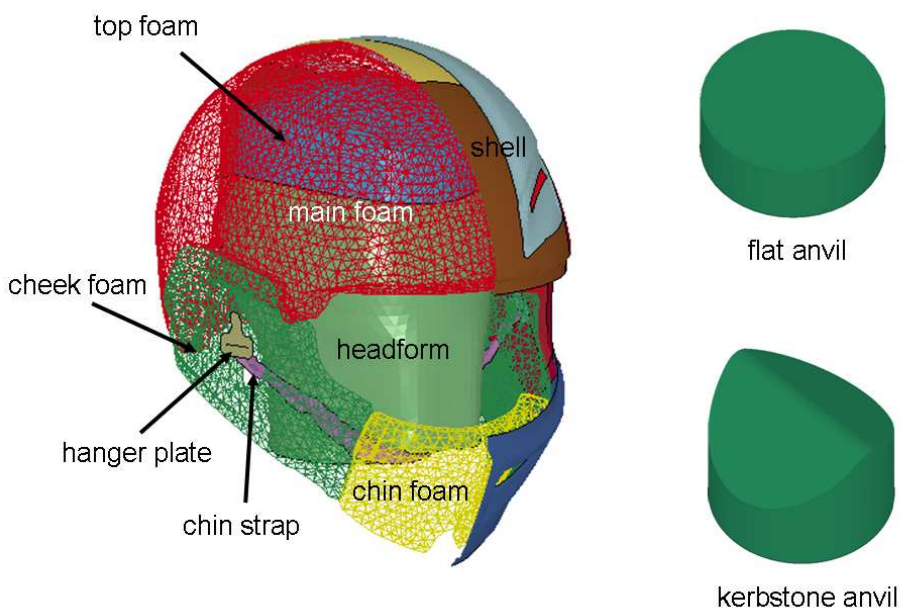


Figure 3 Modelled parts of the helmet (only half of the shell is shown) and anvils.

2.1.6 Contact

Contact was defined at headform/liner, liner/liner, shell/liner, chin strap/headform, chin strap/liner and shell/anvil interfaces using the automatic contact algorithm of LS-DYNA with penalty formulation (Hallquist, 2007). Sliding at the interfaces was modelled using the Coulomb friction model with equal static and dynamic friction coefficients. Cernicchi et al. (2008) used a friction coefficient of 1 for the liner/liner interface and a friction coefficient of 0.5 for the shell/liner and headform/liner interfaces. The friction coefficient at the shell/anvil interface was found 0.55 when the anvil was covered with an abrasive paper (Mills, et al., 2009). Since we did not use an abrasive paper in our tests, a lower value (0.3) was assigned to it in our model. For the chin strap/headform interface, a friction coefficient of 0.5 was employed.

2.1.7 Helmet drop tests

To validate the FE model of the helmet, AGV-T2 helmets were drop tested using a “J” size headform. Drop tests onto a flat anvil were carried out by Dainese S.p.A according to the UNECE 22.05 standard and the results, including resultant linear acceleration of the headform versus time, were given to us for impacts at the B, P, R and X points. Only one test result was available for each impact point, so it was not possible to investigate the repeatability of the tests.

Some drop tests were performed onto a kerbstone anvil at TRL (Transport Research Laboratory, Bracknell, UK). The repeatability of tests with a flat anvil is usually much better than with a kerbstone anvil. Hence, for testing the helmet against a kerbstone anvil, three samples for each impact point were used. The impact points (B, P, R and X) were marked on the helmets with the aid of a reference headform and a fixture equipped with laser pointers and rulers. After positioning the helmet on the headform, the peripheral vision field angles were checked by using a purpose-built gauge shown in Figure 4. Then, the chin strap was tightened.

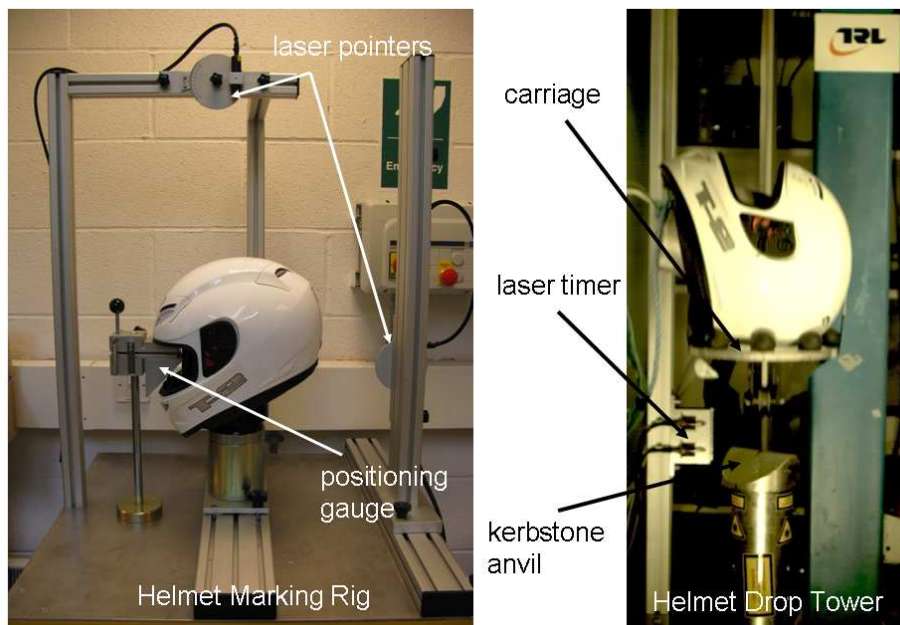


Figure 4 Helmet marking and drop test rigs

The helmeted headform was dropped onto the kerbstone anvil by using the TRL's helmet drop tower shown in Figure 4. The drop height was adjusted so that the impact velocity just before helmet/anvil contact was approximately 7.5 m/s. In each test, this velocity was measured with a laser timer; its variation was not more than 1%. Three orthogonal piezoelectric accelerometers were mounted inside the headform near point G to measure the acceleration with a sampling rate of 100 kHz. All impacts were recorded with a high speed camera at 1000 frames per second.

2.2 Results

The drop tests of the helmet onto the flat and kerbstone anvils were simulated by using the FE model of the helmet. The impact speed was 7.5 m/s and the impact points were B, P, R and X. The simulation results are compared to experimental data in Figure 5 to Figure 8. Generally, the FE prediction is good. For impacts onto the flat

anvil, only one set of data was available. Nonetheless, good repeatability of tests using the kerbstone anvil implies that with the flat anvil the repeatability should also be good.

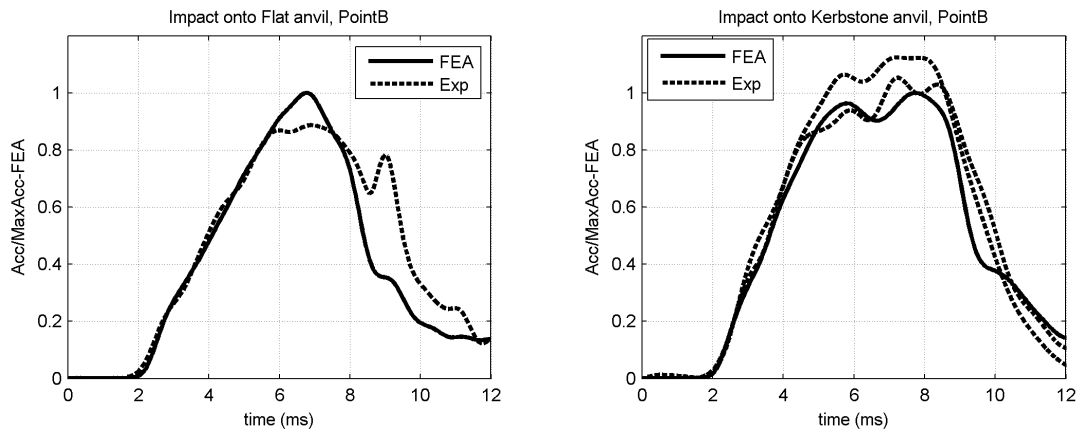


Figure 5 Results of drop tests at point B

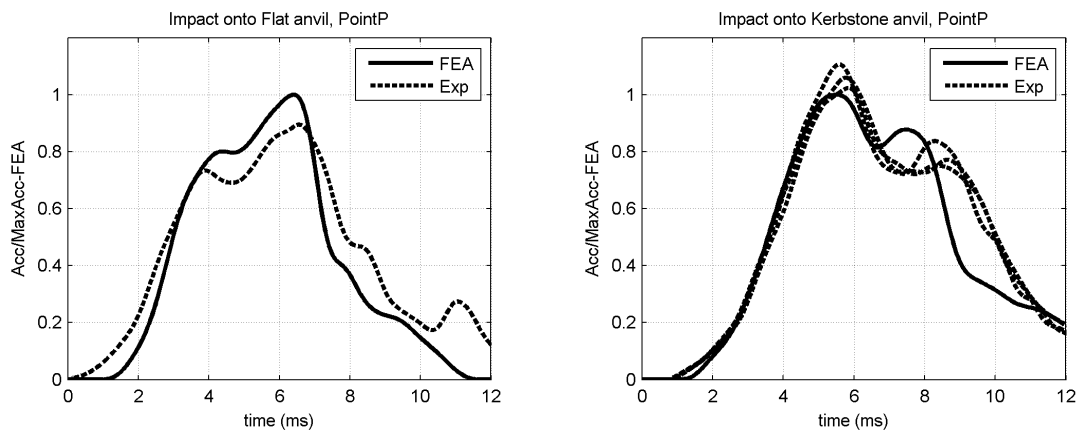


Figure 6 Results of drop tests at point P

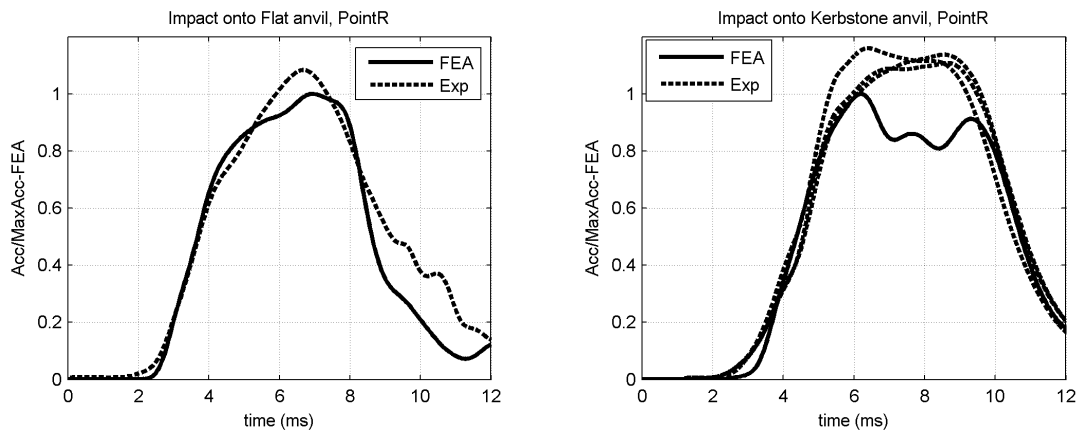


Figure 7 Results of drop tests at point R.

The unloading part (when acceleration descends) of the majority of FE curves has a steeper slope compared to experimental curves. This is probably related to the unloading assumption adopted for developing the foam material model MAT63. In this material model, the unloading occurs on a line whose slope is equal to Young's modulus (E) of the foam (Hallquist, 2007). However, if the slope of the stress-strain curve in the densification region is greater than E (an example is the curve shown in Figure 1), the software increases E to avoid self-intersection of the curve upon unloading from any point in the densification region. For instance, E was increased as much as 100 times in our simulations. Increasing the Young modulus does not probably affect the results in loading as the elastic region is small compared to the plateau region, but it can result in unrealistically steep unloading.

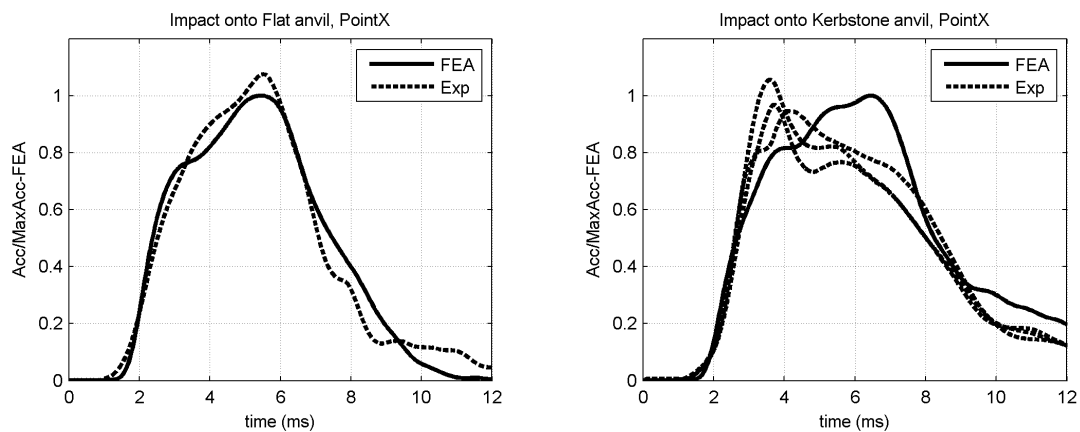


Figure 8 Results of drop tests at point X.

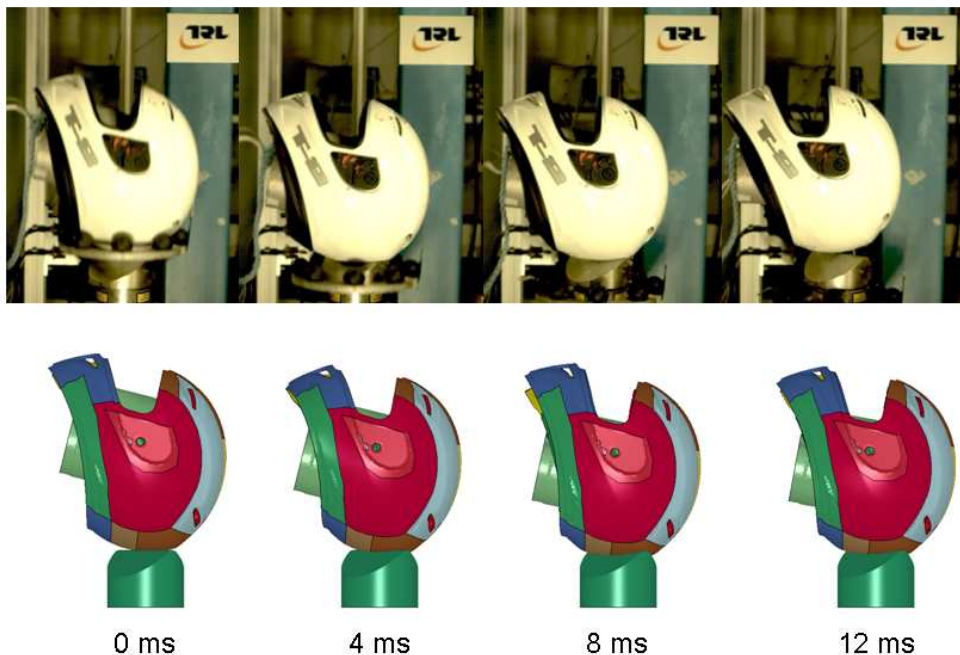


Figure 9 Snapshots of an impact onto kerbstone anvil at point R.

The discrepancy between FE and experimental results is quite remarkable for impacts onto the kerbstone anvil at point R. The larger area under the experimental curves indicates a greater change in the impact velocity, which implies that the headform rebounded earlier in experiments than in simulations. The snapshots shown in Figure 9 indicate that also the helmet rebounded earlier in experiments. These observations indicate that the portion of the internal energy, which was stored in the shell and converted into kinetic energy, was larger in experiments. In other words, the lower FE predicted acceleration can be attributed to the larger portion of the internal energy, which was dissipated through failure of the shell in simulations.

2.3 Discussion

Literature survey indicated that several attempts have been made to model motorcycle helmets with FEM. However, the developed models were rarely validated against experimental drop tests at different impact sites and by using non-flat anvils. Cernicchi and co-workers' paper was found to be the only study that has reported the validation of a model of a helmet for various impact conditions. Our study is analogous to their work. We modelled a commercially available full-face helmet and simulated impacts at B, P, R and X points using both flat and kerbstone anvils. The results were in good agreement with the experimental results which were either provided by the manufacturer or obtained through impact testing the helmet.

There were some noticeable discrepancies between FE predicted and experimental results when a kerbstone anvil was used. The discrepancies were mainly attributed to the larger amount of energy dissipated by the shell through fracture in FEA. The FE model of the shell can be improved in some ways. As explained earlier, the material properties of layers of the shell were found in open literature or by using analytical equations. Better properties may be obtained by carrying out coupon tests on these materials. In addition, using the lay-up that has been used to mould the shell can improve the model.

Another issue is sensitivity of properties of composite materials to the rate of loading. Mechanical properties of carbon and Kevlar epoxy composites are rate-independent in fibre dominated modes, but those of glass epoxy composites enhance with increasing the loading rate (Matthews and Rawlings, 1994). In addition, in matrix dominated modes, including shear related failure, composites with an epoxy resin show strain-rate enhancement. The material model used for the shell in this study does not have the capability to include the strain-rate effect. The energy based material model developed by Iannucci and Ankersen (2006) includes the strain-rate enhancement. However, it is not implemented in LS-DYNA software yet. In addition, there is no data available about the relevant properties of the composites used for the shell. Once such models are available in LS-DYNA, the impact response of composite shell helmets should also be studied by using them.

3 Helmet Full-body Normal Impact Test Using the Hybrid III Dummy

It was shown in the introduction that probable consequences of using a detached headform and, therefore, excluding the rest of the body in the impact absorption test, have not been addressed completely. In this study, we have further investigated these consequences by using an FE model of the Hybrid III dummy. This dummy was chosen because it was used in previous similar studies (COST327, 2001, HIC-Workshop, 2005). In addition, it was available for conducting a set of drop tests in order to validate the FE model of the helmeted dummy.

In this section, the FE model of the dummy is described and validated against experimental results. In order to investigate possible influences of the body on impact responses of the head and helmet, two types of virtual tests are compared: drop test of a helmeted dummy and the drop test of its helmeted detached head. An analytical model of the helmeted headform drop test is explained. The solution to this model enables us to find possible ways to include these influences in the impact absorption test with limited changes to currently used test apparatus.

3.1 Methodology

3.1.1 FE model of the Hybrid III dummy

The family of Hybrid III dummies has been developed by General Motors Corporation for investigating injuries of car occupants in high-speed frontal impacts. This dummy has a flexible neck made of rubber cylinders separated with aluminium discs (Figure 10). Through the centre of this column runs a steel cable. The neck is attached to the head with a revolute joint (Occipital Condyle), whose axis is normal to the coronal plane. At the other end, it is rigidly attached to a rigid steel thoracic spine (the main upper part of the back).

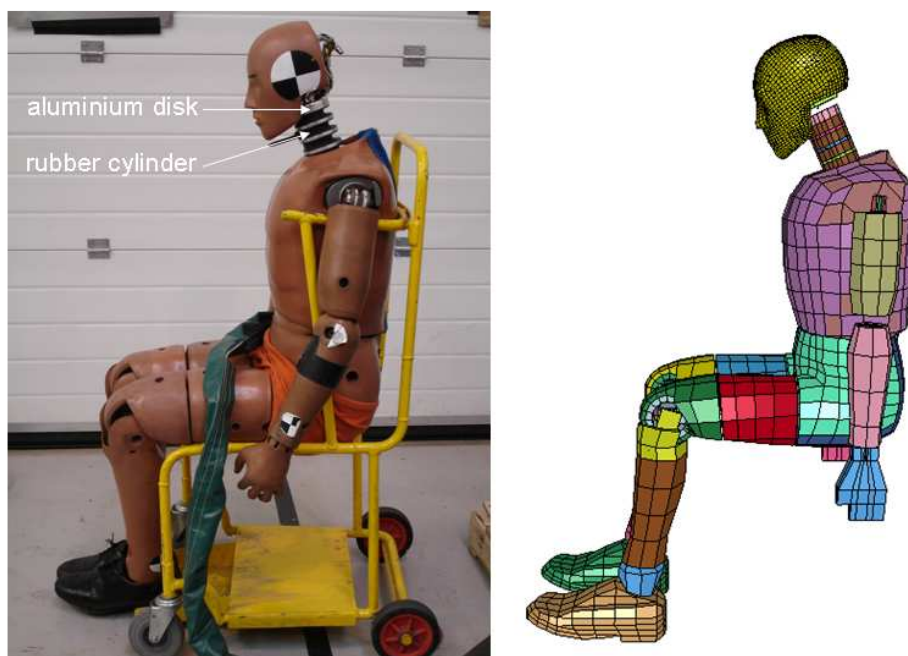


Figure 10 Hybrid III dummy (left) and its FE model (right).

Project: MRTN-CT-2006-035965 MYMOSA

Deliverable 3.4: Virtual and experimental testing of helmets

An FE model of the dummy, which was developed by Livermore Software Technology Corporation (LSTC, 2008) and provided free of charge for LS-DYNA users, was employed in this research (LSTC.H3.103008_v1.0, Figure 10). This model has 7444 nodes and 4295 elements composed of 2648 solid, 1636 shell, 3 beam and 8 discrete elements. The mesh of the head's skin was very coarse compared to the mesh of the helmet liner. Using a CAD file of the skin, a finely meshed FE skin including 3704 hexahedral elements (compared to 136 elements of the original FE skin) was created.

In the model of the dummy, the rubber cylinders of the neck are modelled with spherical joints connecting rigid disks together. The elastic and damping properties of the rubber cylinders are modelled with angular stiffness and angular damping implemented in these joints. The response of the FE model of the neck has been investigated and validated through simulating neck extension and flexion tests of the FMVSS 572 standard (FMVSS572, 1986, Guha, et al., 2008). These tests do not include direct impacts on the head, which can apply a compressive force on the neck while in helmet drop tests the head is exposed to direct impacts. Hence, the performance of the FE model of the dummy was studied and validated through simulating helmet drop tests using the dummy, as explained later.

The dummy was in sitting posture (Figure 10). According to accident investigations (COST327, 2001, MAIDS, 2004), in motorcycle accidents the most frequent collision partners are passenger cars. In an impact with a car, the motorcyclist usually hits the car shortly after motorcycle/car collision, which means the rider does not have enough time to change posture considerably. Therefore, using a dummy in the sitting stance represents a number of body positions immediately before the impact.

3.1.2 Full-body and detached-head drop tests

In order to find possible influences of the body on impact responses of the head and helmet, helmet drop tests using the Hybrid III dummy (full-body) were simulated and compared with the simulation of drop tests in which only the detached head of the dummy was used. To set up the impacts, requirements of the UNECE 22.05 regulation were followed. The skin of the dummy's head was switched to rigid for these impacts.

The FE model of the AGV-T2 helmet was positioned on the dummy's head and its detached head so that the upward field of vision (which is an angle between the horizontal vision line and a line connecting an eyeball to the upper edge of the helmet) was approximately 7°. The front edge of the helmet was displaced towards the rear by 25 mm to follow the instructions of UNECE 22.05. After positioning, there was a small gap (less than 8 mm) between the head and liner, which is filled in the real helmet with the comfort liner.

The head/liner and shell/anvil interfaces were defined using the automatic contact definition of LS-DYNA with the soft constraint penalty formulation (Hallquist, 2007). For a rubber skin/liner interface, Mills et al. (2009) obtained a friction coefficient of 0.5, which was implemented in our FE model. For the shell/anvil interface, a friction coefficient of 0.23 was used. This value was found by dividing the peak tangential force by the peak normal force applied on the anvil, which were recorded in experimental drop tests.

The axis of the dummy's body was horizontal and the orientation of the detached head was exactly the same as the orientation of the dummy's head (Figure 11). In this configuration, the impact occurred near point B. An accident investigation (COST327, 2001) showed that 43% of motorcyclists impacted the opposite object at body impact angles (the angle between the body longitudinal axis and the surface of the opposite object) in the range of 0°-15°. In addition, more than 23% of the helmets were impacted in the frontal side. Therefore, the impact configuration shown in Figure 11 represents a considerable percentage of real-world accidents.

The impacts were against a flat anvil at two impact velocities, 6 m/s and 7.5 m/s. The former was used in the COST study to perform the same comparison but experimentally. The latter is the velocity adopted by the UNECE 22.05 regulation.

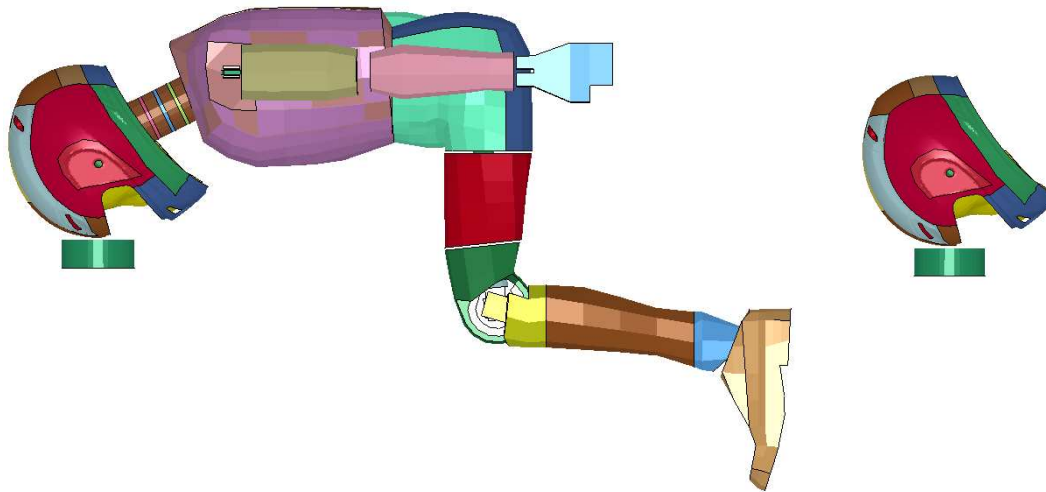


Figure 11 Helmeted Hybrid III dummy (left) and helmeted detached head of the dummy (right) impacting the anvil at point B.

3.1.3 Experimental dummy drop tests

In order to validate the FE model of the helmeted dummy, a 50th percentile male Hybrid III dummy in the sitting posture was equipped with the AGV-T2 helmet and drop tested at TRL (UK). The helmets were size M (57-58) and provided by Dainese S.p.A (Italy). They were positioned on the dummy's head considering the peripheral vision requirements of UNECE 22.05 and the chin strap was fastened with a normal force. The neck of the dummy was calibrated before tests as per the FMVSS 572 (1986) standard and recalibrated after 16 tests to make sure that its response remained in the relevant standard corridors.

For these tests, flat and kerbstone anvils were employed. The anvils were fixed to a load-cell which was fixed to a steel base using bolts and nuts (Figure 12). The rigidity of the base and fixation was very important, because any small natural frequency could interfere with the load and acceleration measurements. The base was constructed of a heavy steel table supported by two beams. The table and beams were hold together by four G-clamps at one end. At the other end, the beams were fastened to the ground. Any air gap between the beams and the ground could decrease the natural frequency of the base; this space was packed up with steel shims.

The dummy was suspended in the air with two slings. The slings were hold (through an auto lock gate carabineer) by the closed jaws of a bomb release attached to the hook of an overhead crane (Figure 13). The drop height (the vertical distance between the impact point on the helmet and the corresponding point on the anvil) was adjusted by the crane and checked with a height ruler, as shown in Figure 14. Lifting the dummy could cause its rotation so that the impact points on the anvil and the helmet were not on a vertical line. This could affect the repeatability of experiments when a kerbstone anvil was used. With the aid of a plump bob, the position of the impact point on the helmet relative to that on the anvil was checked and, if necessary, adjusted (Figure 14).

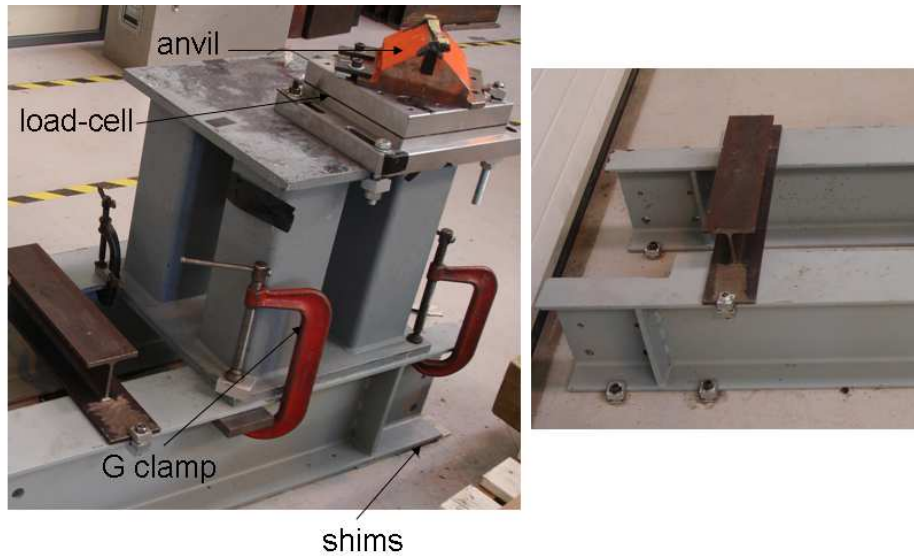


Figure 12 Base, load-cell and anvil (left) and connection of beams to the ground (right).

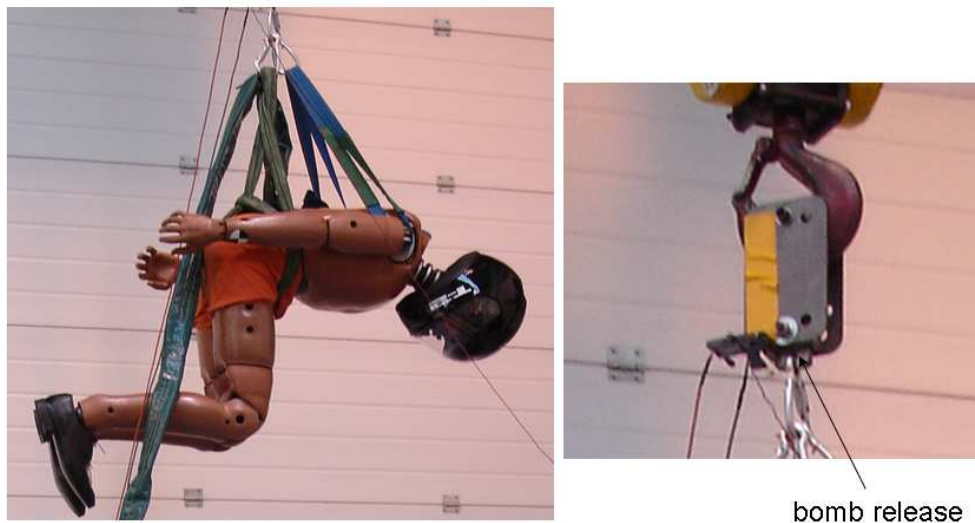


Figure 13 The suspended dummy (left) and the bomb release (right).

The dummy was dropped in front, rear and side impact configurations, as shown in Figure 15. In the front impact, the body axis was horizontal and the sagittal plane was vertical. In the rear impact, owing to the flexibility of the lumbar spine, the body axis made an angle of 26° with the horizontal direction under the gravity load, but the sagittal plane was vertical. For the side impact configuration, the coronal plane was horizontal. In all configurations, the head was displaced under the gravity load owing to the flexibility of the neck.

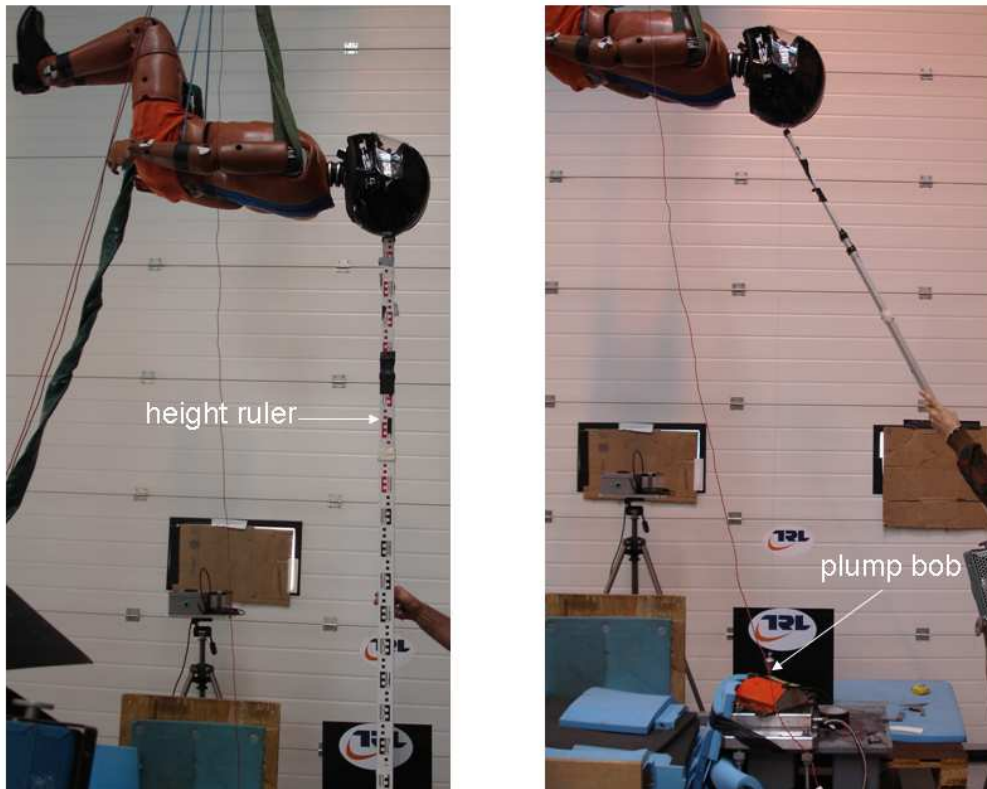


Figure 14 Adjustment of the drop height (left) and the impact point (right).

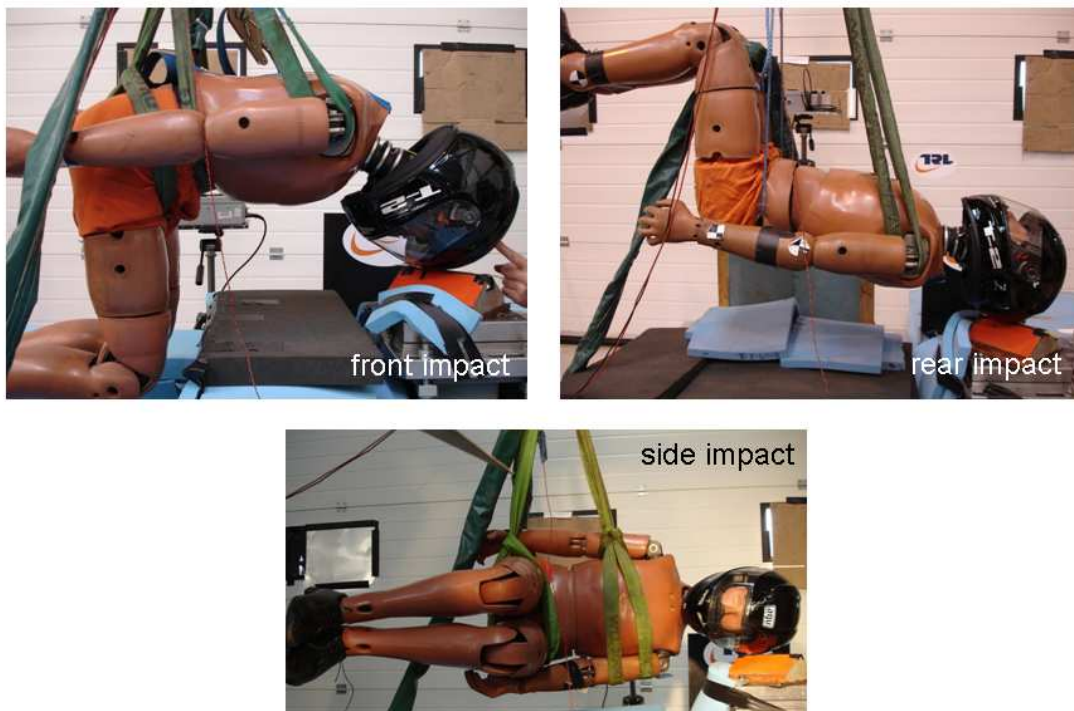


Figure 15 Impact configurations.

Deliverable 3.4: Virtual and experimental testing of helmets

The Hybrid III dummy is not biofidelic in side impacts because the Occipital Condyle joint of this dummy is a revolute joint with an axis normal to the coronal plane while in the human body, this joint has more degrees of freedom. Despite of this fact, the Hybrid III dummy has been used before for side impacts (COST327, 2001, Pang, et al., 2009). In this research, the side impacts were carried out in order to collect a complete set of experimental data for the helmeted dummy. The results will be used to validate the FE model of the helmeted dummy although this model will not be used to compare full-body and detached-head drop tests in the side impact configuration.

The impact velocity for all tests was 6 m/s, which is less than the impact speed set in UNECE 22.05. It was chosen to reduce the risk of damaging the dummy. In a free fall, the height at which an object reaches this speed from zero is 1835 mm. A laser timer was installed to measure the speed of the dummy just before the helmet contacts the anvil. Two reflective strips were attached to a plate mounted on a suitable part of the dummy. The distance between the leading edges of the strips was 100 mm. The laser beam was adjusted to point on the upper strip when the helmet was in contact with the anvil (Figure 16). The timer started when the leading edge of the lower strip cut the beam and stopped when the same edge of the upper strip cut the beam. Since in a free fall the speed of an object increases with a g (gravity) rate, the impact velocity is calculated from the following relation:

$$V = \frac{d}{\Delta t} + \frac{g\Delta t}{2}$$

where d is the distance between the leading edges of the reflective strips and Δt is the time measured by the timer.

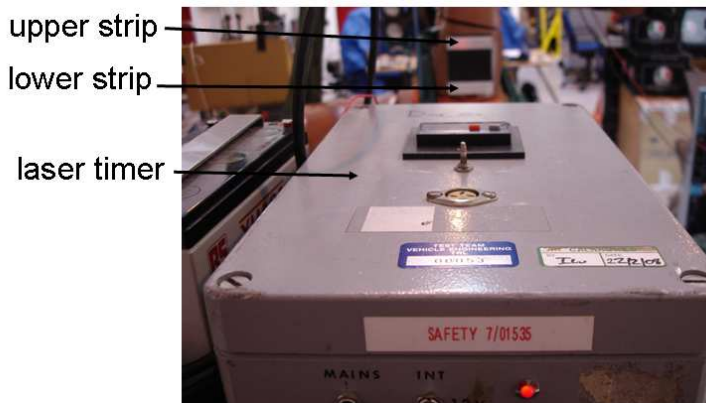


Figure 16 Speed measurement.

The head of the dummy was instrumented with a nine accelerometers package (NAP) in a 3-2-2-2 array (Figure 17). This array, which was first proposed by Padgaonkar et al. (1975), allows for calculating the three components of the rotational acceleration of the head using the outputs of the accelerometers. A standard load-cell was mounted at the Occipital Condyle joint to measure forces and moments at this joint. Another load-cell was located under the anvil to measure the normal and tangential components of the impact force. In total, 18 channels were connected to a DTS data logger. The data acquisition frequency was 38 kHz. A high speed video camera was used to film the impacts at 500 frames per second.

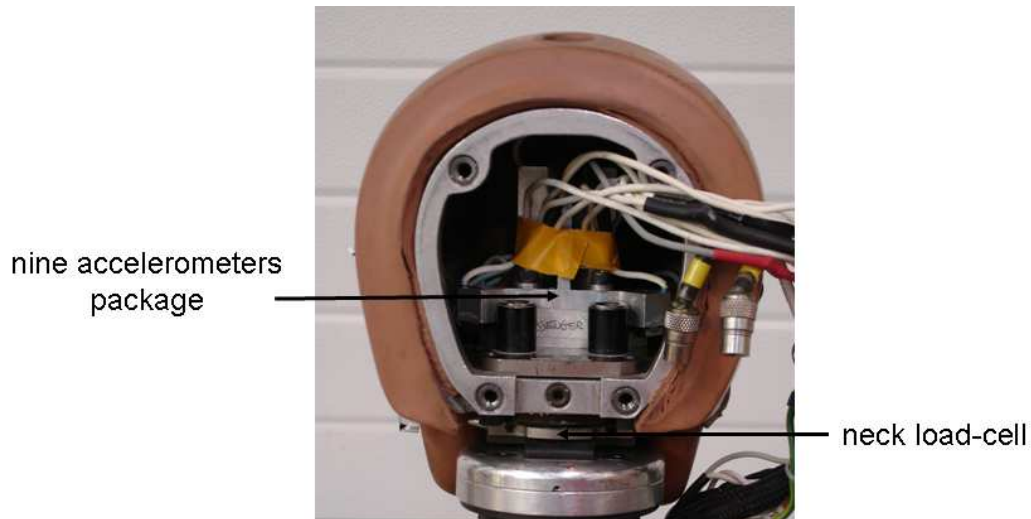


Figure 17 Head and neck instrumentation.

3.2 Results

3.2.1 Experimental dummy drop tests

The recorded data were filtered with a Butterworth filter order 4 at an 800 Hz cut-off frequency. In Table 4, the maximum value of the resultant head linear acceleration ($|a|_{max}$) and the normal force at the anvil/helmet interface ($F_{N,max}$) are reported. The rotational acceleration of the head had two peaks (or valleys). The first peak, which was associated with the loading phase (explained later), is reported in this table. Figure 18 illustrates the positive direction of the head angular acceleration and moment components. The 123 frame is an inertia frame and the xyz frame is fixed to the head. The neck force and moment were measured in the latter.

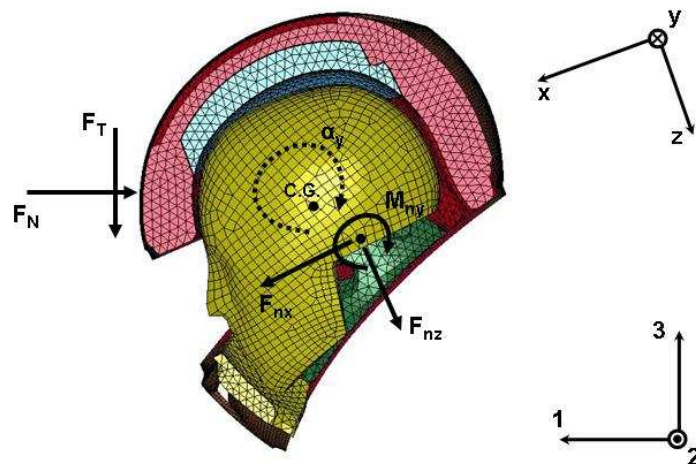


Figure 18 Positive directions of angular acceleration and force and moment components (only half of the helmet is shown).

Table 4 also presents the mean values, standard deviations (SD) and coefficient of variations (CV). As can be seen, the data are more scattered when a kerbstone anvil is used. The

Deliverable 3.4: Virtual and experimental testing of helmets

coefficients of variation of $|a|_{max}$ and $F_{N,max}$ are less than 10% for all impacts except the side impact on kerbstone anvil. This can be attributed to the added complexity of the system by using a kerbstone anvil. In addition, for side impacts more data scatter was expected owing to the irregular shape of the shell and attachments of the visor and chin strap to the shell.

Table 4 Results of dummy drop tests

Impact Configuration		Front		Rear		Side	
Anvil		Flat	Kerb	Flat	Kerb	Flat	Kerb
Number of tests		3	4	4	4	4	5
$ a _{max}$ (g)	Mean	121.1	113.3	122	108.8	162.8	161
	SD ³	1.6	8.3	3.9	4.7	11.5	20
	CV ⁴ (%)	1.3	7.4	3.2	4.3	7.1	12.6
α_x^1 or α_y^2 (krad/s ²)	Mean	4542	3792	-6358	-7169	8027	7381
	SD	412	443	386	1315	535	583
	CV (%)	9.1	11.7	6.1	18.3	6.7	7.9
$F_{N,max}$ (kN)	Mean	6.9	6.1	6.5	5.5	8.9	9.2
	SD	0.0	0.6	0.2	0.1	0.5	0.7
	CV (%)	0.7	9.9	3.3	2.2	6.2	7.7
M_{nx}^1 or M_{ny}^2 (N.m)	Mean	105.7	88.3	-51.3	-29.3	-59.3	-59.6
	SD	4.0	19.9	13.2	16.4	5.8	10.1
	CV (%)	3.8	22.6	25.7	56.1	9.7	16.9

- 1) side impact
- 2) front and rear impacts
- 3) standard deviation
- 4) coefficient of variation

For all impacts, the variation of the rotational acceleration was less than 10%, except the front and rear impacts onto the kerbstone anvil. The rear impact resulted in high deviations of the angular acceleration and neck moment. Analysis of the high speed camera movies revealed that in two of four rear impacts onto the kerbstone anvil, the helmet collided the anvil at a point slightly away from the expected impact point (which is the lowest point on the helmet), as shown in Figure 19. The same phenomenon was detected for the front impacts on the kerbstone anvil shown in the same figure. A slightly displaced impact point did not affect the linear acceleration or the normal force but it influenced the neck moment and the rotational acceleration of the head. It can be concluded that the repeatability of the tests was very good with respect to the linear acceleration and normal force, and it was acceptable in connection with other parameters when a flat anvil was used.

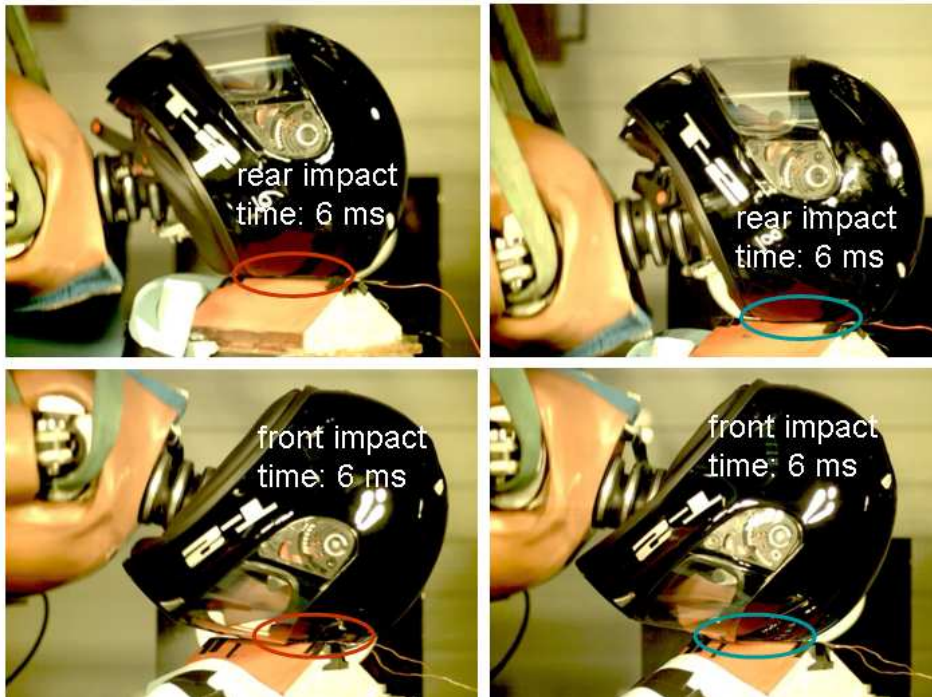


Figure 19 Snapshots showing slightly missed impacts (left) and accurate impacts (right).

3.2.2 Validating the FE model of the dummy

As mentioned before, when the dummy was hoisted, it deformed under the gravity force owing to the flexibility of its neck and lumbar spine. The vertical displacement of the centre of gravity of the head was small for front and side impact configurations, but it was approximately 130 mm for the rear impact configuration. In order to simulate the experiments precisely, FE model of the helmeted dummy was prepositioned. Gravity was applied to the helmeted dummy FE model while the dummy was supported at its waist (and chest for front and side impacts). During these prepositioning simulations, the fine meshed parts of the helmet and dummy were switched to rigid so as to increase the time step. The time step was 4.86 μ s eventually.

After prepositioning, the contacts between the waist (and the chest for front and side impacts) and the supports were deleted and the parts that had been switched to rigid were switched back to deformable. Then, an initial impact speed of 6 m/s was applied to the dummy and helmet. Six simulations including impacts onto flat and kerbstone anvils at front, rear and side sites were performed. Figure 20 shows FEA results of the front impact onto a flat anvil compared with the experimental results.

As can be seen in Figure 20, the head angular acceleration has two peaks. The first peak obtained by the FEA is considerably less than the experimental peaks. It can be attributed to the higher magnitude of the FE predicted neck compressive force, F_{nz} . The dummy's neck is made of rubber cylinders separated by aluminium discs representing vertebrae. However, in the FE model of the dummy the rubber cylinders were replaced with spherical joints, which were not flexible under axial loading and induced a higher compressive force at the head/neck joint. The postponed peak of the anvil force can also be attributed to this difference.

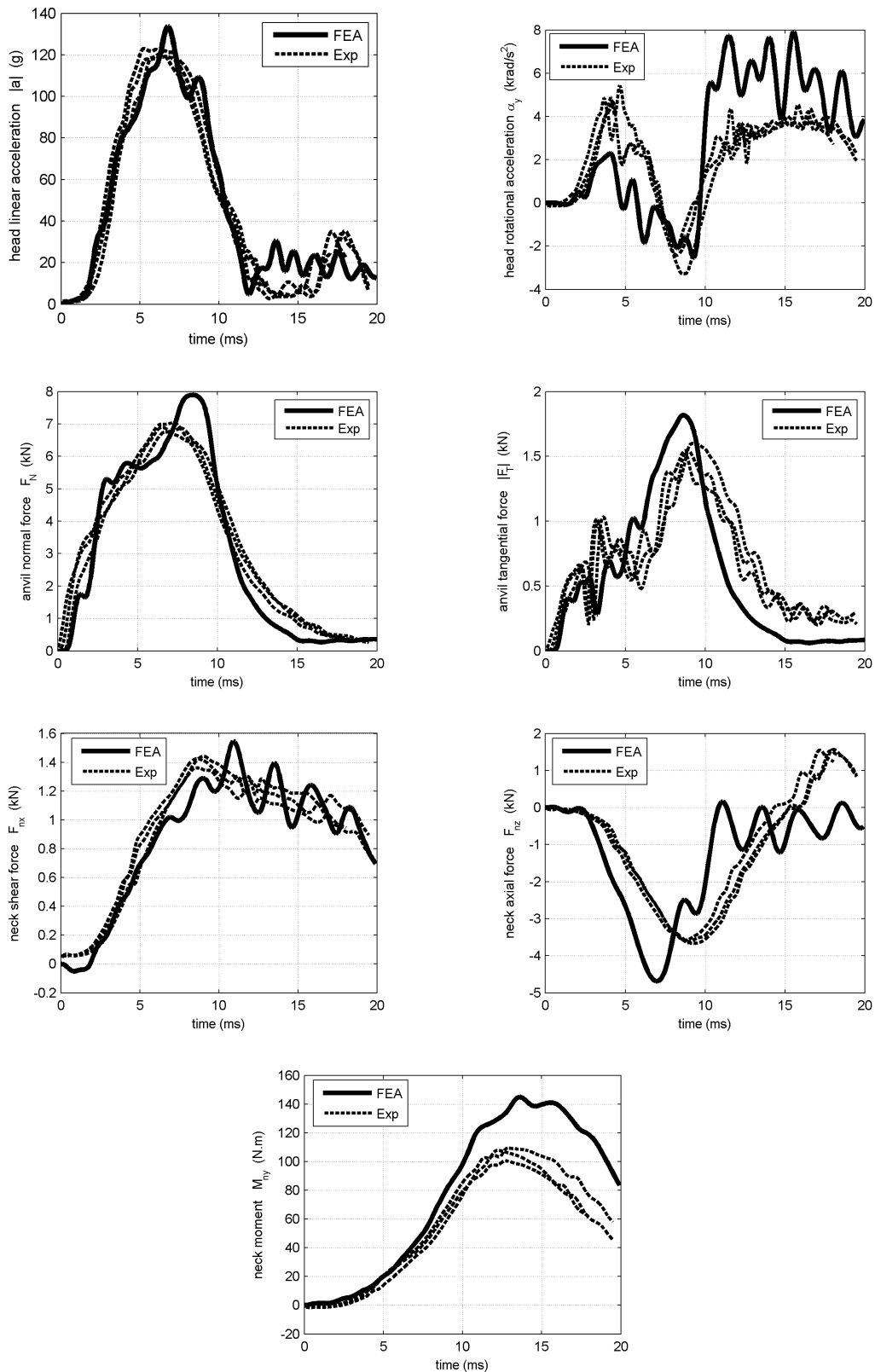


Figure 20 FEA results of the AGV-T2 helmet front impact onto a flat anvil at a 6 m/s impact velocity using a Hybrid III dummy compared with the experimental results for the same impact, shown as dashed curves.

Crushing of the helmet decelerated the head with a growing contact force up to 8 ms. Meanwhile, the body continued its movement owing to its relatively large mass, as shown in Figure 21. The head/body relative movement produced a high moment on the head. A decrease in the head contact force after helmet crushing resulted in the second peak of the angular acceleration under the head/neck moment. Since the peak of the FEA head/neck moment is noticeably higher than the experimental peaks, the second peak of the head angular acceleration is also higher. Decreasing the rotational stiffness of the neck joints can decrease this peak.

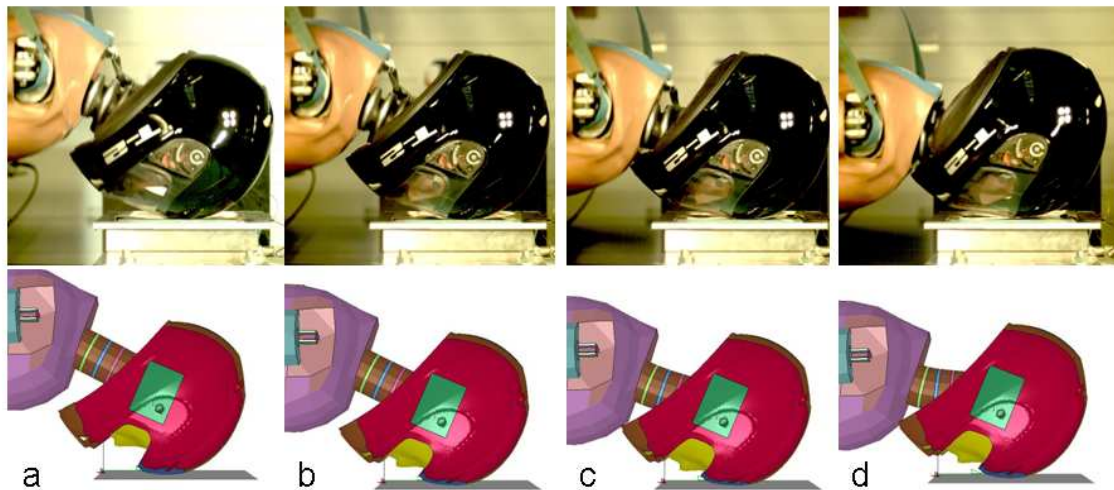


Figure 21 Movement of the body in the front impact test, compared with the FEA; a) 0 ms, b) 4 ms, c) 8 ms and d) 12 ms.

The influence of the body on helmet drop test results is the consequence of the forces and moments which are applied on the head through the neck. When studying this influence, the focus should be on the loading phase because helmets absorb energy in this phase. The comparisons given in Figure 20 and Table 4 indicate that the FE model of the helmeted dummy tends to give good predictions in various impact configurations, at least in the loading phase.

3.2.3 Full-body vs. detached-head drop tests

As mentioned before, the FE models of the Hybrid III dummy and its detached head were equipped with the AGV-T2 helmet and dropped onto a flat anvil at point B. In Figure 22, the head resultant linear acceleration ($|a|$) and the helmet/head interface contact force in the direction normal to the anvil pointing towards the head (F_{hN}) are plotted for drop tests at 6 m/s. As shown in this figure, F_{hN} was increased as a result of the presence of the body, but its maximum value was still less than the threshold of the skull fracture, 10 kN. Another consequence of including the body was a decrease in $|a|$, which can be related to the component of the neck force that acts on the head in the direction opposite to F_{hN} . The value of this force is probably dependent on the stiffness of the neck and the inertia of the rest of the body. The comparisons shown in Figure 22 are consistent with those reported in COST 327 for similar drop tests.

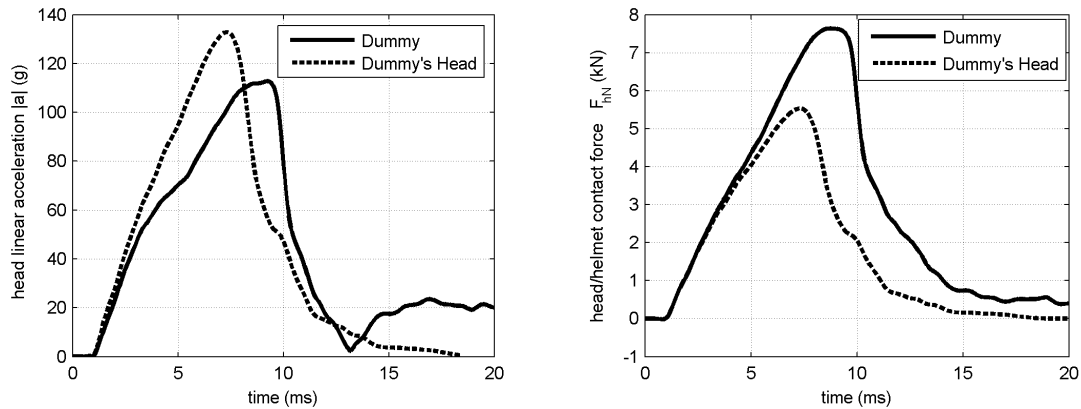


Figure 22 Results of full-body and detached-head drop tests at 6 m/s.

The crushing distance of the liner (Δh) is an impact output which is of a very high importance because it can indicate the probability of bottoming out of the liner. This parameter was not reported in previous full-body impacts due probably to the limitations of experimental studies. In our study, to calculate Δh , the initial clearances at the head/liner, liner/shell and shell/anvil interfaces were subtracted from the maximum displacement of the head normal to the anvil. As presented in Table 5, Δh was larger when the dummy was used.

Table 5 Results of drop test simulations

Impact Type	V_0 (m/s)	$ a _{,max}$ (g)	HIC	$F_{hN,max}$ (kN)	$\Delta h_{,max}$
Detached-head	6	133	597	5.5	27
	7.5	216	1274	8.9	34
Full-body	6	113	499	7.6	33
	7.5	278	1613	17.2	38
Modified Detached-head	6	123	487	7.4	33
	7.5	265	1523	16.0	38

The results of the dummy drop test at 7.5 m/s are plotted in Figure 23. This figure shows that the linear acceleration of the head rises suddenly after 6 ms and exceeds that of the detached head. This is in contrast to the behaviour shown in Figure 22 and that reported in previous experimental studies (Aldman, et al., 1976, Aldman, et al., 1978a, Aldman, et al., 1978b, COST327, 2001). This phenomenon is the consequence of the bottoming out of the foam liner. Increasing the impact speed from 6 m/s to 7.5 m/s caused more deformation of the liner such that its maximum compressive strain in the crushed region was 91% (using a thickness of 42 mm) for the dummy drop test. As reported in Table 5, the head acceleration exceeded the limit set in the UNECE 22.05 (275 g) and the force applied on the head was far larger than the skull fracture threshold. We can conclude that the energy absorption capacity of the helmet was not sufficient for the drop test at 7.5 m/s using the dummy.

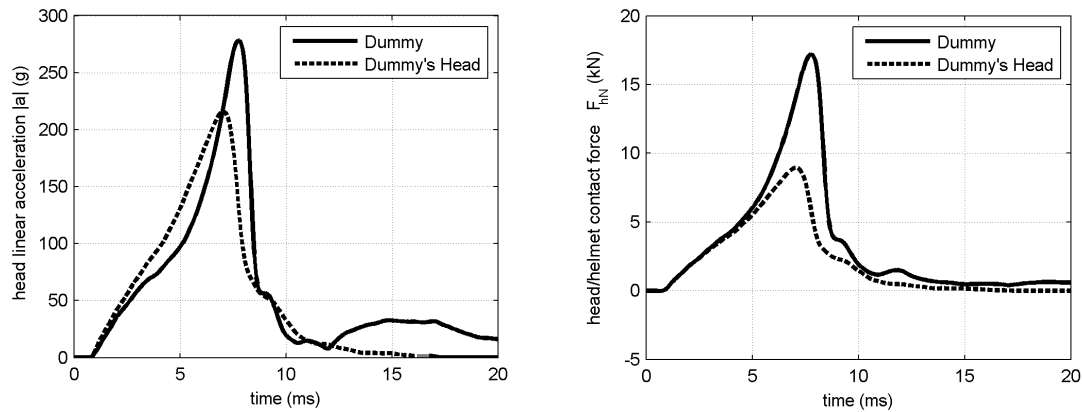


Figure 23 Results of full-body and detached-head drop tests at 7.5 m/s.

The helmet liner is usually designed to reach a maximum compressive strain, when drop tested according to standard procedures, which is not in the densification region of its compressive stress-strain curve in order to avoid bottoming out. Current standards employ a headform in drop tests, while real-world accidents are full-body and as it was shown the liner is compressed more in full-body than detached-head drop tests. This implies that the current helmet standards underestimate the liner crushing distance. Now the question is how the standard test method can be modified to include the effect of the body. To answer this question, an analytical model was proposed for the standard drop test. This model is explained in the next section.

3.2.4 Analytical Model of standard drop test

FE models of helmet drop tests provide detailed outputs for a specific helmet in completely defined impact conditions, whereas a suitable analytical model can provide insights into the relations between impact initial and boundary conditions and its outputs. In this section, an analytical model of the impact response of helmeted headforms is explained. This model results in simple closed-form equations, revealing the relations between input and output parameters. These equations will be used to investigate possible ways of modifying the standard drop test method in order to take into account the effect of the body.

Two parts of a helmet absorb impact energy: the liner and shell. The liner is usually made of expanded polystyrene (EPS), whose typical stress-strain curve has a wide plateau region. Gilchrist and Mills (1994) assumed a constant yield stress (S_y) for the liner under compression and derived the following relation between the normal force on the helmet (F_N) impacting a flat anvil, and the central deflection of the liner (y):

$$F = 2\pi R S_y y \quad (6)$$

The helmet was assumed to be locally spherical with radius R . For impacts onto kerbstone or spherical anvils, this radius should be replaced with an equivalent radius using the relation between equivalent curvatures. For instance, for the impact of a helmet with a local radius of R_h onto a spherical anvil with a radius of R_a , we have:

$$\frac{1}{R} = \frac{1}{R_h} + \frac{1}{R_a}$$

Eq. (6) was found to give a good approximation of the impact behaviour of thin-shelled helmets such as bicycle helmets. The relatively stiff shell of motorcycle helmets can increase the contact area for impacts with kerbstone or spherical anvils. This effect can be taken into account by increasing R , as shown in (Gilchrist and Mills, 1994).

Another function of the shell of a motorcycle helmets is to absorb part of the impact energy. Its contribution to energy absorption is usually 10 to 30% (Shuaeib, et al., 2002), which is a considerable portion. Absorption of the kinetic energy by the shell reduces the speed of the helmet and headform. Therefore, it can be assumed that the impact of a helmet onto an anvil is equivalent to the same impact but at a reduced impact velocity when the shell is removed. To calculate the reduced impact velocity, the energy conservation principle is employed as follows:

$$\frac{1}{2} mV_0^2 = IE_{shell} + IE_{liner} \quad (7)$$

where m is the mass of the helmet and headform and IE is the internal energy (combination of the elastic energy and dissipated energy) at the instance that the velocity is zero just before rebounding. Using the ratio of the total internal energy to the internal energy of the liner (α), the above equation can be written as:

$$\frac{1}{2} mV_0^2 = \alpha IE_{liner} \quad (8)$$

or

$$IE_{liner} = \frac{1}{2} m \left(\frac{V_0}{\sqrt{\alpha}} \right)^2 \quad (9)$$

Thus, the reduced impact velocity ($V_{0,r}$) is:

$$V_{0,r} = \frac{V_0}{\sqrt{\alpha}} \quad (10)$$

By replacing the impact velocity with the reduced impact velocity, we can ignore the shell in our model. We also assume that the liner and headform are one rigid body whose centre of

gravity is located at the centre of gravity of the headform. By using Newton's second law and substituting for force from eq. (6), we have:

$$m\ddot{y} = -2\pi RS_y y \quad (11)$$

The earth's gravity is not considered in this equation as it is negligible compared to the accelerations expected in helmet drop tests. Assuming $y(0)=0$, the solution to the differential eq. (11) is:

$$y(t) = \frac{V_{0,r}}{\omega} \sin \omega t, \quad \omega = \sqrt{\frac{2\pi RS_y}{m}} \quad (12)$$

The derivation of the peak linear acceleration of the headform (a_{max}), the maximum normal force on the anvil ($F_{N,max}$) and the maximum compression of the liner (Δh_{max}) is straightforward from eqs. (6), (11) and (12):

$$a_{max} = \frac{V_{0,r}}{\sqrt{m}} \sqrt{2\pi RS_y} \quad (13)$$

$$F_{N,max} = \sqrt{m} V_{0,r} \sqrt{2\pi RS_y} \quad (14)$$

$$\Delta h_{max} = \frac{\sqrt{m} V_{0,r}}{\sqrt{2\pi RS_y}} \quad (15)$$

The head linear acceleration in eq. (13) is equivalent to the resultant acceleration ($|a|$) since the model has only one translational degree of freedom.

Eqs. (13), (14) and (15) may not be used for final design of helmets but they can provide very useful information about the relation between impact inputs, main properties of the helmet and impact outputs. For example, they predict that in order to decrease the acceleration of the headform by 20% the yield stress of the foam (which is a function of its density) should be decreased by about 36%. In addition, the thickness of the liner should be increased because with this change its crushing distance will be increased by about 25%. These equations are used in the next section to suggest how the standard helmet drop test can be modified in order to take into account the important effect of the body.

3.2.5 Modified Headform

It was shown that the presence of the whole body in helmet drop tests results in further crushing of the liner. Therefore, when a helmet is designed to pass a standard drop test using a headform, its liner may bottom out when the whole body is present in the same impact conditions. This indicates the important role of the body, which should be considered in energy absorption tests. Since using a dummy in helmet drop tests has a drastic impact on the price of helmets, other measures should be adopted.

Deliverable 3.4: Virtual and experimental testing of helmets

The results given in Table 5 indicate that when the liner was not loaded beyond its energy absorption capacity ($V_0 = 6$ m/s), $|a|_{max}$ was lower using the dummy, but $F_{hN,max}$ and Δh_{max} were greater compared to the detached-head drop test. Referring to eqs. (13), (14) and (15), the only modification to the helmeted headform impact inputs that influences the outputs in the same way is increasing the mass of the headform.

The increased mass of the headform can be estimated with a simple approach. From Newton's second law for the rigid head of the dummy in the direction normal to the anvil, we have:

$$F_{hN}/a_N = -F_{nN}/a_N + m_h \quad (16)$$

where F_{nN} is the head/neck joint force and m_h is the mass of the head. The subscript N refers to the component in the direction normal to the anvil pointing towards the head. $-F_{nN}/a_N$, which has a positive value in the loading phase, has the dimension of mass. It can be interpreted as a mass that should be added to the mass of the head if the rest of the body is removed in order to maintain F_{hN}/a_N at the same level. In other words, $-F_{nN}/a_N$ is the contribution of the body through the neck to generating higher F_{hN}/a_N . $-F_{nN}/(m_h a_N)$, a dimensionless parameter, is the ratio of the added mass to the mass of the head, which will be denoted by γ_m . This parameter, called "the added mass index", can be used for evaluating the influence of the body through the neck on the responses of the head and helmet in drop tests.

Figure 24 plots γ_m for the helmeted Hybrid III dummy virtual drop test at 7.5 m/s. As shown in this figure, γ_m varies slightly until the peak of acceleration occurs. Then, it increases with a steep slope as the acceleration falls towards zero. The value of γ_m at the peak of the head acceleration, 0.43, was chosen to calculate an increased mass for the detached head of the dummy. The detached head of the dummy was modified by increasing its mass and mass moment of inertia components by $\gamma_m = 0.43$, and it was virtually drop tested with the helmet in the same impact conditions. From the definition of the added mass index, it was expected that the drop test of the modified detached head of the dummy in these impact conditions will give similar results compared to the dummy drop test.

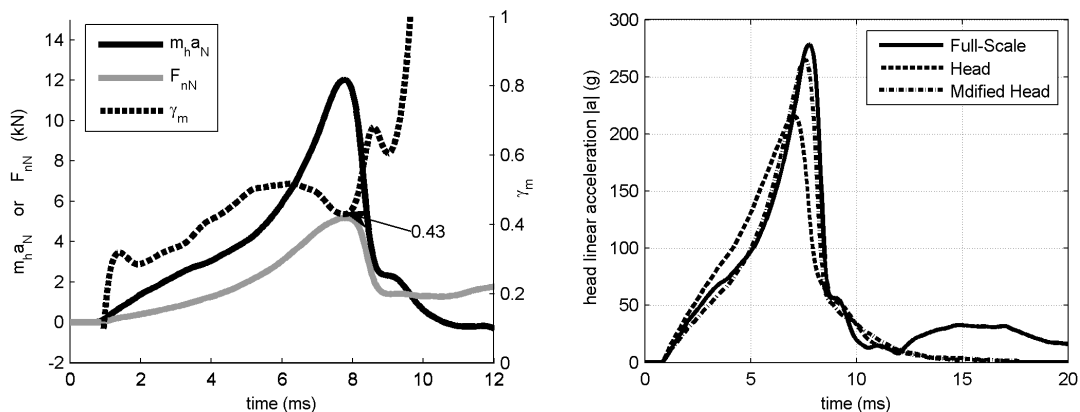


Figure 24 Added mass index for the helmeted dummy drop test (left) and comparison of the results using $\gamma_m=0.43$ (right); at a 7.5 m/s impact velocity.

Figure 24 compares $|a|$ between the full-body, modified detached-head and detached-head drop tests. The time history of the head acceleration obtained from the modified detached-head drop test compares well with that of the dummy drop test, which is remarkable because it is acknowledged that both the acceleration level and its dwell time are indicators of head injury. As a result, HIC , which is a function of linear acceleration vs. time, was predicted with a less than 3% error as presented in Table 5. $F_{hN,max}$, which is an indicator of the skull fracture, was also predicted precisely using the modified detached head. The most important impact output, Δh_{max} , was also replicated successfully by using the modified detached head. These evidences indicate that a suitable value was selected for the added mass index for the given impact conditions.

3.3 Discussion

A validated FE model of the Hybrid III dummy equipped with the FE model of a commercially available helmet was used to simulate full-body helmet drop tests. The results were compared to the results of the same impacts but by using the detached head of the dummy. It was shown that including the whole body in the drop tests reduced $|a|_{max}$ when the foam liner at the crushed region did not enter the densification region of its characteristic stress-strain curve, but it increased $F_{hN,max}$ and Δh_{max} . These results are similar to the experimental findings reported in COST (2001) for an impact velocity of 6 m/s, except for the crushing distance of the liner, which was not reported in this reference. An increase in the impact velocity from 6 m/s to 7.5 m/s caused complete bottoming out of the liner in the dummy drop test and consequently the very high contact force and head acceleration. These results raise doubts about standard helmet testing procedures, which employ a headform.

Using a dummy to drop test helmets is cumbersome and would have a drastic impact on their price. A simple and economical way of including the effect of the body in drop tests is to use a headform but to change one (or more) impact conditions. The closed-form equations suggested that increasing the mass of the headform can replicate the influence of the body on $|a|_{max}$, $F_{hN,max}$ and particularly Δh_{max} . The comparison between the results of drop tests using the dummy and its detached head modified by increasing its mass confirmed this hypothesis.

Another impact condition that may be changed is the impact velocity. Increasing this parameter, however, does not affect all the outputs in the same way as increasing the headform mass does. Eqs. (13), (14) and (15) indicate that an increase in the impact velocity increases $F_{hN,max}$ and Δh_{max} , but it also augments $|a|_{max}$. This change may be implemented in the standard drop test method but it should be accompanied by increasing the acceptance limit of $|a|_{max}$; otherwise helmets cannot be designed and optimized so that their whole capacity will be used in protecting the head. To clarify this point, the dummy drop test at 6 m/s is compared to the detached-head drop test at 7.5 m/s. As presented in Table 5, the crushing distance of the liner was the same in both impacts, but $|a|_{max}$ and HIC were approximately two times higher in the detached-head impact. It may be argued that the limits set for these injury indicators in the standards are already increased¹. However, this implies that helmets designed to pass these standards are efficient at an impact velocity lower than the adopted impact velocity. For instance, helmets certified by UNECE 22.05 are probably efficient at a 6 m/s impact speed for impacts at point B. It should be mentioned that this conclusion is based on using the Hybrid III dummy as a surrogate for the human body.

Using a heavier headform with the same limit of the head linear acceleration can cause helmet manufacturers to use stiffer foams with higher yield stress; a conclusion that can easily be drawn from eq. (13). However, there might be some real-world impact conditions in which head almost completely decouples from the body, for instance when the body is

¹ In fact this is true with respect to HIC . The acceptance limit of HIC in UNECE 22.05 is 2400, while the threshold of serious head injuries (AIS3) is 1500.

Deliverable 3.4: Virtual and experimental testing of helmets

stopped by an obstacle before the head impacts another object. Consequently, a helmet that has passed the new test method may induce higher head decelerations due to its stiffer liner as compared to a helmet approved by the current standard test. Consider a helmet that has been designed to pass the new test method so that the peak linear acceleration of the headform in a drop test is equal to the limit of the head linear acceleration (A). For this helmet, from eq. (13), we have:

$$A = \frac{V_{0,r}}{\sqrt{(1 + \gamma_m)m_h + m_{helmet}}} \sqrt{2\pi R S_Y} \quad (17)$$

In impact conditions for which the head decouples from the body, γ_m becomes zero. If the impact speed and site are the same as those of the standard drop test, the right hand side of the above equation becomes larger than A . To avoid such a design, the head linear acceleration limit set in the standard should be decreased to:

$$A' = A / \sqrt{\frac{(1 + \gamma_m)m_h + m_{helmet}}{m_h + m_{helmet}}} \quad (18)$$

With this modified limit, the new design of the helmet has to satisfy the following equation:

$$A = \frac{V_{0,r}}{\sqrt{m_h + m_{helmet}}} \sqrt{2\pi R S_Y} \quad (19)$$

where γ_m is not involved anymore. This limit should be reduced the most when $m_{helmet} \ll m_h$, which results in $A' = A / (1 + \gamma_m)^{0.5}$. For $\gamma_m = 0.43$, $A' = 0.84A$.

Only decreasing the limit of acceleration cannot replicate the influence of the body in headform drop tests. This change probably results in using softer and thicker foams in helmets, but still the crushing distance of the liner is underestimated due to employing a headform in helmet drop tests. In other words, a helmet that has passed the headform drop test with a decreased limit of acceleration may bottom out when the headform is replaced by the whole body.

The value that was obtained for the added mass index was based on using the Hybrid III dummy as a surrogate for the whole body. This dummy was developed to study car frontal impacts, in which the head is under indirect loading. Some researchers believe that this dummy is not suitable for investigating direct impacts to the head, such as motorcycle accidents, because its neck is too stiff (Herbst, et al., 1998). This issue will be investigated by using a very detailed FE model of the human body in similar impacts.

4 Conclusions

A commercially available helmet was modelled in LS-DYNA and validated against standard drop tests onto both flat and kerbstone anvils. The FE model of the helmet was virtual drop tested by using the Hybrid III dummy and its detached head. It was shown that the presence of the body increases the crushing distance of the liner compared to the tests with the headform. This effect caused complete bottoming out of the liner at a 7.5 m/s impact speed

Project: MRTN-CT-2006-035965 MYMOSA

Deliverable 3.4: Virtual and experimental testing of helmets

and consequently the large head acceleration and normal force. Using the solution to the analytical model of the helmet drop test and the FEA results, it has been shown that increasing the mass of the headform can be a simple yet appropriate way of including the effect of the whole body in drop tests.

Project: MRTN-CT-2006-035965 MYMOSA

Deliverable 3.4: Virtual and experimental testing of helmets

References

1. ACEM, ACEM's view on PTW fatality statistics in Europe. 2006.
2. Aiello, M., Galvanetto, U., and Iannucci, L., Numerical simulations of motorcycle helmet impact tests. *International Journal of Crashworthiness* 12, 2007, 1-7.
3. Aldman, B., Lundell, B., and Thorngren, L., Non-perpendicular impacts, an experimental study on crash helmets. *IRCOBI*, 1976, 322-331.
4. Aldman, B., Lundell, B., and Thorngren, L., Helmet attenuation of the head response in oblique impacts to the ground. *IRCOBI*, 1978a, 118-128.
5. Aldman, B., Lundell, B., and Thorngren, L., Oblique impacts, a parametric study in crash helmets. *IRCOBI*, 1978b, 129-141.
6. Becker, E. B., *Helmet Development and Standards*. In: Yoganandan, N., Pintar, F. A., Larson, S. J., and Sances, A., (Eds.). IOS Press, 1998.
7. Cernicchi, A., Galvanetto, U., and Iannucci, L., Virtual modelling of safety helmets: practical problems. *Int. J. of Crashworthiness* 13, 2008, 451-467.
8. Chang, C. H., Chang, L. T., Chang, G. L., Huang, S. C., and Wang, C. H., Head injury in facial impact - A finite element analysis of helmet chin bar performance. *Journal of Biomechanical Engineering-Transactions of the Asme* 122, 2000, 640-646.
9. Chang, L. T., Chang, C. H., and Chang, G. L., Fit effect of motorcycle helmet - A finite element modeling. *Jsmc International Journal Series a-Solid Mechanics and Material Engineering* 44, 2001, 185-192.
10. Cook, R. D., *Concepts and applications of finite element analysis*. Wiley, New York, NY, 2001.
11. COST327, *Motorcycle safety helmets, final report of the action*. 2001.
12. Di Landro, L., Sala, G., and Olivieri, D., Deformation mechanisms and energy absorption of polystyrene foams for protective helmets. *J. Polym. Test.* 21, 2002, 217-228.
13. FMVSS572, Subpart E - Hybrid III Test Dummy, *Federal Motor Vehicle Safety Standards, USA*, 1986.
14. Ghajari, M., Caserta, G. D., and Galvanetto, U., *Comparison of safety helmet testing standards*. 2008.
15. Gibson, L. J., and Ashby, M. F., *Cellular Solids*. Cambridge University Press, 1999.
16. Gilchrist, A., and Mills, N. J., Modeling of the Impact Response of Motorcycle Helmets. *Int. J. Impact Eng.* 15, 1994, 201-218.
17. Gilchrist, A., and Mills, N. J., Protection of the side of the head. *J. Accid. Anal. and Prev.* 28, 1996, 525-535.
18. Guha, S., Bhalsod, D., and Krebs, J., *LSTC Hybrid III Dummies: Positioning and Post-Processing*. 2008.
19. Hallquist, J. O., *Ls-Dyna keyword user's manual*. Livermore Software Technology Corporation, 2007.
20. Hallquist, J. O., *Ls-Dyna theory manual*. Livermore Software Technology Corporation, 2007.
21. Herbst, B., Forrest, S., Chng, D., and A. Sances, J., Fidelity of anthropometric test dummy necks in rollover accidents. *16th International Technical Conference on the Enhanced Safety of Vehicles, Windsor, Canada*, 1998.
22. HIC-Workshop, *Final report of workshop on criteria for head injury and helmet standards*. 2005.
23. HyperWorks, 9.0 Release. Altair, 2008.

Project: MRTN-CT-2006-035965 MYMOSA

Deliverable 3.4: Virtual and experimental testing of helmets

24. Iannucci, L., and Ankersen, J., An energy based damage model for thin laminated composites. *Composites Science and Technology* 66, 2006, 934-951.
25. Kostopoulos, V., Markopoulos, Y. P., Giannopoulos, G., and Vlachos, D. E., Finite element analysis of impact damage response of composite motorcycle safety helmet. *J. Compos. : Part B* 33, 2002, 99-107.
26. LSTC, Livermore Software Technology Corp., 2008.
27. MAIDS, MAIDS final report 1.2: in-depth investigations of accidents involving powered two wheelers. 2004.
28. Matthews, F. L., and Rawlings, R. D., *Composite materials : engineering and science*. Chapman & Hall, London ; New York, 1994.
29. Mills, N. J., and Gilchrist, A., Finite-element analysis of bicycle helmet oblique impacts. *Int. J. Impact Eng.* 35, 2008, 1087-1101.
30. Mills, N. J., Wilkes, S., Derler, S., and Flisch, A., FEA of oblique impact tests on a motorcycle helmet. *Int. J. Impact Eng.* 36, 2009, 913-925.
31. NCSA, Traffic safety facts: Bodily injury locations in fatally injured motorcycle riders. 2007.
32. Pang, T. Y., Thai, K. T., and McIntosh, A. S., Head and neck dynamics in helmeted Hybrid III impacts. IRCOBI, York, UK, 2009.
33. Shuaeib, F. M., Hamouda, A. M. S., Hamdan, M. M., Umar, R. S. R., and Hashmi, M. S. J., Motorcycle helmet - Part II. Materials and design issues. *J. Mater. Process. Technol.* 123, 2002, 422-431.
34. Soden, P. D., Hinton, M. J., and Kaddour, A. S., Lamina properties, lay-up configurations and loading conditions for a range of fibre-reinforced composite laminates. *Composites Science and Technology* 58, 1998, 1011-1022.
35. UNECE22.05, Uniform provisions concerning the approval of protective helmets and of their visors for drivers and passengers, United Nations, 2002.
36. Yettram, A. L., Godfrey, N. P. M., and Chinn, B. P., Materials for Motorcycle Crash Helmets - a Finite-Element Parametric Study. *Plastics Rubber and Composites Processing and Applications* 22, 1994, 215-221.